ATLAS PUB Note
ATL-PHYS-PUB-2018-048
15th December 2018

Prospects for searches for staus, charginos and neutralinos at the high luminosity LHC with the ATLAS Detector

The ATLAS Collaboration

The current searches at the LHC have yielded sensitivity to weakly-interacting supersymmetric particles in the hundreds of GeV mass range and the reach at the high-luminosity phase of the LHC is expected to significantly extend beyond the current limits. This document presents example benchmark studies for stau pair production ($\tilde{\tau}^+\tilde{\tau}^-$) using a final state with two hadronically decaying taus, chargino pair production ($\tilde{\chi}_1^+\tilde{\chi}_1^-$) using a final state with two leptons, and chargino-neutralino production ($\tilde{\chi}_1^\pm\tilde{\chi}_2^0$) using either a $\ell\ell\ell$ or ℓbb final state. A parameterised simulation of the ATLAS detector at a centre-of-mass energy of 14 TeV is used. Expected results are shown for an integrated luminosity of 3000 fb^{-1}, where the discovery regions exceed the current limits on SUSY particle masses set at the LHC by hundreds of GeV. The discovery potential at the HL-LHC reaches stau masses of 530 GeV and chargino masses of 660 GeV, for $\tilde{\tau}^+\tilde{\tau}^-$ and $\tilde{\chi}_1^+\tilde{\chi}_1^-$ production, respectively. For $\tilde{\chi}_1^\pm\tilde{\chi}_2^0$ production, the discovery region reaches up to 920 GeV (1080 GeV) in $\tilde{\chi}_1^\pm$ and $\tilde{\chi}_2^0$ masses, where the $\tilde{\chi}_2^0$ decays via the Standard Model Z (h) boson. The 95% CL expected exclusion potentials at the HL-LHC reach $\sim$ 200 GeV higher in mass than the discovery potentials for all cases considered.

ATL-PHYS-PUB-2018-048
16 December 2018

1 Introduction

Supersymmetry (SUSY) [1–6] proposes that for every boson (fermion) of the Standard Model (SM) there exists a fermionic (bosonic) partner. The scalar superpartners of the SM fermions are called sfermions (comprising the charged sleptons, $\tilde{\ell}$, the sneutrinos, $\tilde{\nu}$, and the squarks, $\tilde{q}$), while the gluons have fermionic superpartners called gluinos ($\tilde{g}$). The bino, wino and higgsino fields are fermionic superpartners of the SU(2)×U(1) gauge fields of the SM, and the two complex scalar doublets of a minimally extended Higgs sector, respectively. Their mass eigenstates are referred to as charginos $\tilde{\chi}_i^{\pm}$ ($i = 1, 2$) and neutralinos $\tilde{\chi}_j^0$ ($j = 1, 2, 3, 4$), numbered in order of increasing mass. The direct production of charginos, neutralinos and sleptons through electroweak interactions may dominate the SUSY production at the LHC if the masses of the gluinos and squarks are large.

SUSY offers natural solutions to many of the problems with the SM. For example, SUSY particles with masses at the electroweak scale can cancel quadratic divergences to the Higgs mass corrections. SUSY can also accommodate the unification of the gauge interactions and a radiative breaking of the electroweak symmetry. Under the conservation of R-parity [7], the lightest SUSY particle (LSP) is stable and is a good candidate for the dark matter in the universe. Furthermore, the Minimal Supersymmetric Standard Model (MSSM) requires a Higgs boson with mass below ~ 135 GeV which is consistent with the Higgs boson observed at the LHC.

The search for weak-scale SUSY is one of the highest physics priorities for the current and future LHC runs. The high luminosity upgrade of the LHC (HL-LHC) is expected to deliver proton-proton collisions at a centre-of-mass-energy of 14 TeV, with an integrated luminosity of around 3000 fb^{-1}. The large dataset expected at the end of HL-LHC offers an unprecedented discovery potential for heavy SUSY particles in the electroweak sector, of masses around or above a TeV. This note assesses the ATLAS sensitivity at the end of HL-LHC to direct production of various SUSY partners in the electroweak sector including the stau ($\tilde{\tau}$), chargino and neutralinos under the assumption of R-parity conservation.

2 The HL-LHC and the ATLAS detector

In the Run-2 data-taking period, the ATLAS experiment collected 149 fb^{-1} of proton-proton collisions from the LHC at centre-of-mass energies of 13 TeV, with an average number of collisions per bunch crossing of $\langle\mu\rangle = 34$. A second long shutdown (LS2) will follow, during which the injection chain is foreseen to be modified and the accelerator will be able to achieve centre-of-mass-energies of 14 TeV. During LS3, the accelerator is foreseen to be upgraded to the HL–LHC, which is expected to deliver an integrated luminosity of about 3000 fb^{-1}, with an average number of pileup interactions per bunch crossing of $\langle\mu\rangle \sim 200$.

The ATLAS detector [8, 9] is a multi-purpose particle detector with a cylindrical geometry.[1] It consists of layers of inner tracking detectors surrounded by a superconducting solenoid, calorimeters, and a muon

[1] The ATLAS experiment uses a right-handed coordinate system with its origin at the nominal pp interaction point at the centre of the detector. The positive x-axis is defined by the direction from the interaction point towards the centre of the LHC ring, with the positive y-axis pointing upwards, while the beam direction is along the z-axis. Cylindrical coordinates (r, ϕ) are used in the transverse (x, y) plane, ϕ being the azimuthal angle around the beam direction. The pseudorapidity is defined in terms of the polar angle θ from the z-axis as $\eta = -\ln[\tan(\theta/2)]$. The distance in $y - \phi$ space between two objects is defined as $\Delta R = \sqrt{(\Delta y)^2 + (\Delta\phi)^2}$, where y is the rapidity. Transverse energy is computed as $E_{\mathrm{T}} = E \cdot \sin\theta$.

spectrometer, and will need several upgrades [10–15] to cope with the expected higher luminosity at the HL-LHC, the associated high pileup, and the intense radiation environment. The primary motivation for the upgrade design studies is to evaluate the potential of the experiment for searches and measurements despite these harsh conditions. A new inner tracking system, extending the tracking region from $|\eta| \leq 2.7$ up to $|\eta| \leq 4.0$, will provide the ability to reconstruct forward charged particle tracks, which can be matched to calorimeter clusters for forward electron reconstruction, or associated to forward jets. The inner tracker extension also enables muon identification at high pseudorapidities if additional detectors (such as micro-pattern gaseous or silicon pixel detectors) are installed between the endcap calorimeters and the New Small Wheel [16] in the region $2.7 < |\eta| \leq 4.0$. Despite being in an area without magnetic field, such detectors would increase the muon spectrometer acceptance and could be used to identify (tag) inner detector tracks in the forward region as muons, while relying entirely on the inner tracker for the momentum measurement.

3 Electroweak SUSY searches at the HL–LHC

A broad range of electroweak SUSY scenarios and their experimental signatures are considered here, including the two-tau signature from $\tilde{\tau}^+\tilde{\tau}^-$ production in Section 4, the dilepton signature from $\tilde{\chi}_1^+\tilde{\chi}_1^-$ production in Section 5, and the three-lepton and $1\ell bb$ signatures from $\tilde{\chi}_1^\pm\tilde{\chi}_2^0$ production in Section 6. Hadronically decaying taus are used for the $\tilde{\tau}^+\tilde{\tau}^-$ search, while light leptons (e, μ only) are used for the $\tilde{\chi}_1^+\tilde{\chi}_1^-$ and $\tilde{\chi}_1^\pm\tilde{\chi}_2^0$ searches.

The individual analyses follow a coherent approach as much as possible, using the same parameterisations of the upgraded ATLAS detector configuration and the associated experimental uncertainties, the same Monte Carlo (MC) simulations for the common signal and background processes, and the same statistical framework for the interpretation of the results. The definitions of the physics objects follow similar strategies from either earlier publications using data or the previous studies for the HL-LHC. For the signal scenarios considered in this note, most of the final state particles are expected to be in the central region. Therefore the pseudorapidity selections for these final states physics objects remain mostly in the central regions. Signal regions (SR) are typically defined to target one or more regions in the signal model parameter space, using advanced kinematic variables including the output from multivariate methods. Event selections for the signal regions are usually optimised by maximising the expected sensitivity Z_N [17], which takes into account the systematic uncertainties on the background.

The HistFitter [18] software framework is used for the statistical interpretation of the results. In order to quantify the probability for the background-only hypothesis to fluctuate to the observed number of events or higher, a one-sided p_0-value is calculated, where the profile likelihood ratio is used as a test statistic [19]. A signal model can be excluded at 95% confidence level (CL) if the CL_s [20] of the signal-plus-background hypothesis is below 0.05.

Experimental and theoretical uncertainties on the SUSY signal and SM background are accounted for in the exclusion fits. Experimental systematic uncertainties have been estimated based on the expected performance of the upgraded ATLAS detector as documented in Ref. [21]. The theoretical uncertainties, such as the overall cross-section and the modelling of the kinematic shapes, are halved compared to the state-of-art predictions found in Run-2 analyses. The systematic uncertainties arising from the statistics in the control region in data are assumed to scale with the inverse of the square-root of the integrated luminosity. MC-based, statistics-driven sources of uncertainty are considered negligible.

MC simulated event samples are used to predict the background from SM processes and to model the SUSY signal. The effects of an upgraded ATLAS detector are taken into account by applying energy smearing, efficiencies and fake rates to generator level quantities, following parameterisations based on detector performance studies with full simulation and HL-LHC conditions. The effect of the high pileup at the HL-LHC is incorporated by overlaying pileup jets onto the hard-scatter events. Jets from pileup are randomly selected as jets to be considered for analysis with $\sim 2\%$ efficiency, based on the expected performance of a Jet Vertex Tagger at the HL-LHC [21]. The most relevant MC samples have equivalent luminosities (at $\sqrt{s} = 14$ TeV) of at least 3000 fb^{-1}.

SUSY signal samples are generated at leading-order accuracy using MadGraph5_aMC@NLO [22] interfaced to Pythia 8 [23] with the A14 [24] tune for the modelling of the parton showering (PS), hadronisation and underlying event (UE). The matrix element (ME) calculation is performed at tree-level and includes the emission of up to two additional partons. The PDF set used for the generation is NNPDF23LO [25]. The ME–PS matching is done using the CKKW-L [26] prescription, with a matching scale set to one quarter of the mass of the pair produced particles. The cross-sections used to evaluate the signal yields are calculated to next-to-leading order in the strong coupling constant, adding the resummation of soft gluon emission at next-to-leading-logarithmic accuracy (NLO+NLL) [27, 28]. The nominal cross section and the uncertainty are taken from an envelope of cross section predictions using different PDF sets and factorisation and renormalisation scales, as described in Ref. [29].

Background samples were simulated using different MC generators depending on the process. The event generators, the accuracy of theoretical cross-sections, the underlying-event parameter tunes, and the PDF sets used for the background samples are summarised in Table 1. For all samples, except the ones generated using Sherpa [30], the Evtgen v1.2.0 [31] program was used to simulate the properties of the bottom- and charm-hadron decays.

Process	Generator + fragmentation/hadronisation	Tune	PDF set	Cross-section order
W/Z+jets	Powheg-Box v1 [32] + Pythia 8.186 [33] Sherpa 2.2.1 [30]	AZNLO Default	CTEQ6L1 NNPDF30NNLO [34]	NNLO NNLO
$t\bar{t}$	Powheg-Box v2 + Pythia 8.186	A14	NNPDF23LO [25]	NNLO+NNLL
Single top	Powheg-Box v1 or v2 + Pythia 6.428 [35]	Perugia2012 [36]	CT10 [37]	NNLO+NNLL
Diboson (fully leptonic) (semi leptonic)	Sherpa 2.2.1 Powheg-Box v1 + Pythia 8.186	Default AZNLO [38]	NNPDF30NNLO CTEQ6L1	NLO NLO
Triboson	Sherpa 2.2.2	Default	NNPDF30NNLO	NLO
$t\bar{t}+X$	MadGraph 2.2.2 [22] + Pythia 8.186	A14	NNPDF23LO	NLO
Higgs	Powheg-Box v2 + Pythia 8.186	AZNLO	CTEQ6L1	NNLO+NNLL
Multijet	Pythia 8.186	AU2 [39]	CT10	NLO

Table 1: List of MC generators used for the SM background processes. Information is given about the underlying-event tunes, the PDF sets and the pQCD highest-order accuracy (LO, NLO, next-to-next-to-leading order, NNLO, and next-to- next-to-leading-log, NNLL) used for the normalization of the different samples. The Diboson process includes WW, WZ and ZZ. The $t\bar{t}$+X process includes $t\bar{t}$+W, $t\bar{t}$+Z and $t\bar{t}$+WW. For the W+jets process, Sherpa was used in the $(1\ell bb)$ final state, while Powheg+Pythia was used for the other final states. In the direct stau analysis, a combination of generators are used to model the W+jets events, where $W \to e/\mu\nu$ and $W \to \tau\nu$ are modelled with Powheg+Pythia and Sherpa, respectively.

4 Search for direct stau production

Searches for the direct production of light stau pairs at the HL-LHC are motivated by both experimental and theoretical considerations. As of today the most stringent exclusion limits are from LEP, making the search for direct staus a crucial "unturned stone" in the hunt for SUSY at the LHC. Staus are expected to be the lightest slepton flavor in models of GUT scale unification and the lighter stau is favoured to be mostly right-handed. Furthermore, in models with a light stau and lightest neutralino $\tilde{\chi}_1^0$ with a small mass difference, stau co-annihilation processes [40] in the early universe can reduce the $\tilde{\chi}_1^0$ relic density and make it consistent with observations from cosmological measurements [41].

A search for stau production is presented here, which uses a final state with two hadronically decaying τ leptons. Two simplified models describing the direct production of $\tilde{\tau}^+\tilde{\tau}^-$ are used in this document: one considers stau partners of the left-handed τ lepton ($\tilde{\tau}_\mathrm{L}$), and a second considers stau partners of the right-handed τ lepton ($\tilde{\tau}_\mathrm{R}$). In both models, the stau decays with a branching fraction of 100% to the SM τ-lepton and the LSP, which is a common scenario in the phenomenological Minimal Supersymmetric SM [42] when $\tilde{\chi}_1^\pm$, $\tilde{\chi}_2^0$ and $\tilde{\nu}_\tau$ are heavier than the stau. The relevant diagram for this model can be seen in Figure 1.

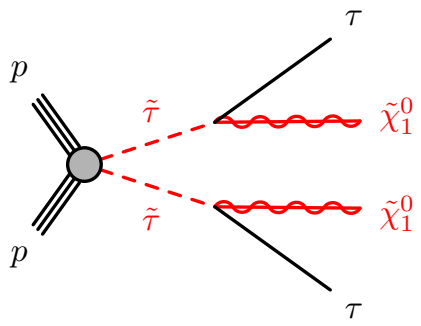

Figure 1: Diagram illustrating the signal scenario considered for the pair production of charged staus targeted by the two-tau final state.

The signature considered here is two hadronically decaying taus, low jet activity, and large missing transverse momentum ($E_\mathrm{T}^\mathrm{miss}$) from the $\tilde{\chi}_1^0$ and neutrinos. The SM background is dominated by W/Z+jets, multi-boson, multi-jet, and top pair production. In the ATLAS Run-1 search for combined $\tilde{\tau}_\mathrm{L}^+\tilde{\tau}_\mathrm{L}^-$ and $\tilde{\tau}_\mathrm{R}^+\tilde{\tau}_\mathrm{R}^-$ production [43], only a narrow range of stau masses ($m(\tilde{\tau}_\mathrm{R}, \tilde{\chi}_1^0) = (109, 0)$ GeV) was excluded due to the very small production cross section. Analysis of the 2015+2016 Run-2 data by CMS [44] did not further extend the sensitivity to direct stau production. Thus, this scenario is an interesting case to study at the HL-LHC, where significant gains in sensitivity could be made.

The event pre-selection is based on that of the previous 8 TeV analysis [43] and 13 TeV analysis [45]. Hadronically decaying taus are selected with $p_\mathrm{T} > 20$ GeV and $|\eta| < 4$, while electrons and muons are selected with $p_\mathrm{T} > 10$ GeV and $|\eta| < 2.47$ ($|\eta| < 2.5$ for muons). Jets are reconstructed with the anti-k_t algorithm [46, 47] with a radius parameter of 0.4, with $p_\mathrm{T} > 20$ GeV and $|\eta| < 4$. Jets are identified as b-jets using the MV2c10 tagging algorithm, operating at an efficiency of 70% in $t\bar{t}$ simulation. To remove close-by objects from one another, an overlap removal based on ΔR is applied.

SM processes where one or more jet is mis-identified as a hadronically decaying tau (fake tau) contribute to the total background. To maximize the available MC statistics, these backgrounds are estimated by

assigning a weight to each jet, where the weight corresponds to the tau fake rate in the HL-LHC detector performance parameterisation. The probability for an event to have one or two fake taus is assessed using all possible combinations of jets, and each event is then weighted by the probability it will contribute to the fake tau background. Cases with more than three fake taus are not considered due to the low probability (less than 10^{-6}).

Before the optimization, pre-selection cuts are applied to suppress the SM background. Events are selected with exactly two tightly identified hadronic taus with $|\eta| < 2.5$, and the two taus must have opposite electric charge (OS). The tight tau algorithm correctly identifies one-prong (three-prong) taus with an efficiency of 60% (45%) and with a light-flavour jet misidentification probability of 0.06% (0.02%). Events with electrons, muons, b-jets or forward jets ($|\eta| > 2.5$) are vetoed. The effect of a di-tau trigger is considered by requiring the leading tau has $p_{\mathrm{T}} > 50\,\mathrm{GeV}$ and the sub-leading tau has $p_{\mathrm{T}} > 40\,\mathrm{GeV}$, with an assumed trigger efficiency of 64%. To suppress the SM background, a loose jet veto is applied that rejects events containing jets with $|\eta| < 2.5$ and $p_{\mathrm{T}} > 100\,\mathrm{GeV}$. Since the SUSY signal involves two undetected $\tilde{\chi}_1^0$, the resulting $E_{\mathrm{T}}^{\mathrm{miss}}$ spectrum tends to be harder than that for the major SM backgrounds, thus $E_{\mathrm{T}}^{\mathrm{miss}} > 200\,\mathrm{GeV}$ is required to reject the multi-jet background. A Z veto is imposed, where the invariant mass of the two taus, $m_{\tau\tau}$, is required to be larger than 100 GeV to suppress contributions from Z/γ^* + jets production. To suppress the top quark and multi-jet backgrounds, the sum of the two-tau transverse mass[2] $m_{\mathrm{T}\tau 1} + m_{\mathrm{T}\tau 2}$, defined using the transverse momentum of the leading (next-to-leading) tau and $E_{\mathrm{T}}^{\mathrm{miss}}$, must be larger than 450 GeV.

The stransverse mass m_{T2} [48, 49] is used to further discriminate SUSY events from SM processes. It can be shown to have a kinematic endpoint for events where two massive pair produced particles each decay to two objects, one of which is detected and the other escapes undetected. It is defined as

$$m_{\mathrm{T2}} = \min_{\vec{q}_{\mathrm{T}}}\{\max\left[m_{\mathrm{T}}(\vec{p}_{\mathrm{T},1},\, \vec{q}_{\mathrm{T}}),\, m_{\mathrm{T}}(\vec{p}_{\mathrm{T},2},\, \vec{P}_{\mathrm{T}}^{\mathrm{miss}} - \vec{q}_{\mathrm{T}})\right]\}, \tag{1}$$

where $\vec{p}_{\mathrm{T},1}$ and $\vec{p}_{\mathrm{T},2}$ are the transverse momentum vectors of the two visible particles, $\vec{P}_{\mathrm{T}}^{\mathrm{miss}}$ is the missing transverse momentum, and $\vec{q}_{\mathrm{T}}$ is the transverse vector that minimises the larger of the two transverse masses m_{T}. A requirement of $m_{\mathrm{T2}} > 35\,\mathrm{GeV}$ is applied to suppress the top, W+jets and Z/γ^* + jets backgrounds.

Starting from this common pre-selection, a cut-and-count method is used to define various SRs. To target signal scenarios with different kinematics, three benchmark points are selected in the optimisation, based on the mass difference between the $\tilde{\tau}$ and $\tilde{\chi}_1^0$, $\Delta m \equiv m_{\tilde{\tau}} - m_{\tilde{\chi}_1^0}$:

- $\Delta m < 150\,\mathrm{GeV}$: $m(\tilde{\tau}, \tilde{\chi}_1^0) = (160, 40)\,\mathrm{GeV}$
- $\Delta m \in [150, 300]\,\mathrm{GeV}$: $m(\tilde{\tau}, \tilde{\chi}_1^0) = (400, 160)\,\mathrm{GeV}$
- $\Delta m \geq 300\,\mathrm{GeV}$: $m(\tilde{\tau}, \tilde{\chi}_1^0) = (500, 1)\,\mathrm{GeV}$

Finally, several kinematic variables that offer good discrimination power between signal and SM backgrounds are used to optimise the SR selection: the p_{T} of the leading and next-to-leading tau, the event $E_{\mathrm{T}}^{\mathrm{miss}}$, the angular separation between the leading and next-to-leading tau $\Delta\phi(\tau 1, \tau 2)$ and $\Delta R(\tau 1, \tau 2)$, the jet veto p_{T} threshold, along with $m_{\mathrm{T}\tau 1} + m_{\mathrm{T}\tau 2}$ and m_{T2}. The selection on these variables is optimized for high Z_N, assuming an uncertainty of 20% on the sum of all backgrounds. This uncertainty is a rough

[2] The transverse mass is defined by $m_{\mathrm{T}} = \sqrt{2 p_{\mathrm{T},i} P_{\mathrm{T}}^{\mathrm{miss}} (1 - \cos\Delta\phi)}$, where $p_{\mathrm{T},i}$ is the transverse momentum vectors of the visible particle i, $P_{\mathrm{T}}^{\mathrm{miss}}$ is the missing transverse momentum, and $\Delta\phi$ is the angle between the particle and the $\vec{P}_{\mathrm{T}}^{\mathrm{miss}}$.

value of the total background uncertainty without the multi-jet uncertainty contributions from the Run-2 studies.

Three signal regions are defined to maximise model-independent discovery sensitivity based on the optimization for scenarios with low (SR-low), medium (SR-med) and high (SR-high) mass differences between the $\tilde{\tau}$ and $\tilde{\chi}_1^0$. Furthermore, another disjoint signal region binned in m_{T2} is defined to maximise model-dependent exclusion sensitivity based on the previous SR-high signal region with the jet veto threshold cut loosened to $p_{\mathrm{T}} > 100\,\mathrm{GeV}$. Each SR is identified by the range of the m_{T2}, and is shown in Table 2. Figure 2 show the distributions of m_{T2} in these signal regions, applying all SR selections with the exception of m_{T2} itself.

Table 2: Summary of selection requirements for the direct stau signal regions.

Common Selection				
exactly two tight taus with opposite sign e/μ veto, b-jet veto $m_{\tau\tau} > 100\,\mathrm{GeV}$ (Z-veto) $E_{\mathrm{T}}^{\mathrm{miss}} > 200\,\mathrm{GeV}$ $p_{\mathrm{T}\tau 2} > 75\,\mathrm{GeV}$ $\Delta R(\tau 1, \tau 2) < 3$ $\Delta\phi(\tau 1, \tau 2) > 2$				
Selection	SR-low	SR-med	SR-high	SR-exclHigh
jet veto threshold	$p_{\mathrm{T\,jet}} > 40\,\mathrm{GeV}$	$p_{\mathrm{T\,jet}} > 40\,\mathrm{GeV}$	$p_{\mathrm{T\,jet}} > 20\,\mathrm{GeV}$	$p_{\mathrm{T\,jet}} > 100\,\mathrm{GeV}$
$p_{\mathrm{T}\tau 1} >$	150 GeV	200 GeV	200 GeV	200 GeV
$m_{\mathrm{T}\tau 1} + m_{\mathrm{T}\tau 2} >$	500 GeV	700 GeV	800 GeV	800 GeV
$m_{\mathrm{T2}}(\tau 1, \tau 2)$	$\in [80\,\mathrm{GeV}, \infty]$	$\in [130\,\mathrm{GeV}, \infty]$	$\in [130\,\mathrm{GeV}, \infty]$	$\in [80\,\mathrm{GeV}, 130\,\mathrm{GeV}]$ $\in [130\,\mathrm{GeV}, 180\,\mathrm{GeV}]$ $\in [180\,\mathrm{GeV}, 230\,\mathrm{GeV}]$ $\in [230\,\mathrm{GeV}, \infty]$

Tables 3 and 4 show the expected numbers of events for the SM backgrounds and three SUSY reference points in the ditau signal regions for an integrated luminosity of 3000 fb^{-1}. Only the statistical uncertainties for signal and backgrounds are shown in Table 3 and Table 4.

The systematic uncertainties are evaluated based on the SR-high systematic uncertainty in Ref. [45], where the dominant background experimental uncertainties in that study are the uncertainty on the multi-jet estimation ($\sim 33\%$), the tau energy scale in situ uncertainty ($\sim 8\%$), the tau energy scale uncertainty from modelling ($\sim 8\%$) and the detector ($\sim 13\%$), the tau ID efficiency uncertainty ($\sim 5\%$), the uncertainty from $E_{\mathrm{T}}^{\mathrm{miss}}$ reconstruction ($\sim 6\%$), and the uncertainty from the jet energy sale ($\sim 4\%$). The dominant signal uncertainties are the tau energy scale in situ uncertainty ($\sim 7\%$), the tau energy scale uncertainty from detector ($\sim 6\%$), the tau ID efficiency uncertainty ($\sim 13\%$), the MC/data related trigger systematics ($\sim 7\%$ in total), and the signal cross-section uncertainty ($\sim 9\%$).

A few of the experimental uncertainties are expected to be smaller at the HL-LHC compared to the 13 TeV studies, as described in Ref [21]. In particular, the tau energy scale insitu uncertainty is scaled

Table 3: Expected numbers of events for the SM background and the three benchmark signal models for combined $\tilde{\tau}_L^+\tilde{\tau}_L^-$ and $\tilde{\tau}_R^+\tilde{\tau}_R^-$ production in the signal regions SR-low, SR-med and SR-high. The "Other SM" contains contributions from the Top, Higgs boson and Multi-jet processes. Entries marked as '-' indicate negligible background contributions (less than 0.1). Uncertainties describe the MC statistical uncertainties only.

	SR-low	SR-med	SR-high
W+jets	8.8 ± 2.8	2.12 ± 0.56	1.00 ± 0.21
Multi-boson	2.6 ± 1.3	0.35 ± 0.18	-
Z/γ^* + jets	1.4 ± 1.0	-	-
Other SM	0.98 ± 0.40	-	-
SM total	13.8 ± 3.3	2.57 ± 0.58	1.10 ± 0.21
$m(\tilde{\tau}_L/\tilde{\tau}_R, \tilde{\chi}_1^0) = (160, 40)$ GeV	34.9 ± 7.2	2.2 ± 1.6	0.63 ± 0.44
$m(\tilde{\tau}_L/\tilde{\tau}_R, \tilde{\chi}_1^0) = (400, 160)$ GeV	24.1 ± 1.6	13.8 ± 1.2	8.3 ± 1.0
$m(\tilde{\tau}_L/\tilde{\tau}_R, \tilde{\chi}_1^0) = (500, 1)$ GeV	19.4 ± 1.5	15.0 ± 1.3	11.6 ± 1.2

Table 4: Expected numbers of events for the SM background and the three benchmark signal points for combined $\tilde{\tau}_L^+\tilde{\tau}_L^-$ and $\tilde{\tau}_R^+\tilde{\tau}_R^-$ production in the exclusion ditau signal regions. The "Other SM" contains contributions from the Top, Higgs boson and Multi-jet processes. Entries marked as '-' indicate negligible background contributions (less than 0.1). Uncertainties describe the MC statistical uncertainties only.

	SR-exclHigh			
m_{T2} [GeV]	[80, 130]	[130, 180]	[180, 230]	[230, ∞]
W+jets	2.42 ± 0.52	1.22 ± 0.26	1.10 ± 0.24	0.54 ± 0.12
Multi-boson	0.49 ± 0.10	0.08 ± 0.02	0.05 ± 0.01	0.04 ± 0.01
Z/γ^* + jets	-	-	-	-
Other SM	0.14 ± 0.03	0.04 ± 0.01	0.03 ± 0.01	0.02 ± 0.00
SM total	3.06 ± 0.44	1.34 ± 0.18	1.19 ± 0.15	0.60 ± 0.06
$m(\tilde{\tau}_L/\tilde{\tau}_R, \tilde{\chi}_1^0) = (160, 40)$ GeV	0.96 ± 0.13	0.63 ± 0.09	0.00 ± 0.00	0.00 ± 0.00
$m(\tilde{\tau}_L/\tilde{\tau}_R, \tilde{\chi}_1^0) = (400, 160)$ GeV	4.79 ± 0.67	9.11 ± 1.28	6.43 ± 0.90	2.97 ± 0.42
$m(\tilde{\tau}_L/\tilde{\tau}_R, \tilde{\chi}_1^0) = (500, 1)$ GeV	1.84 ± 0.26	4.21 ± 0.59	5.99 ± 0.84	7.81 ± 1.10

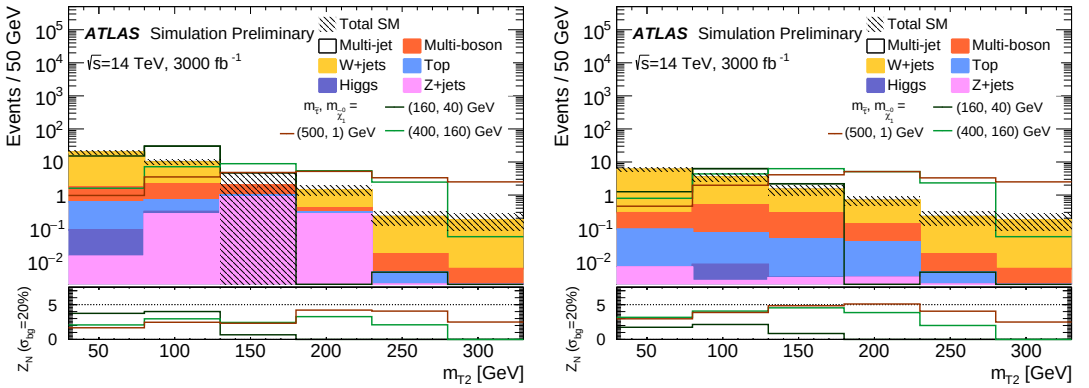

(a) SR-low m_{T2}

(b) SR-med m_{T2}

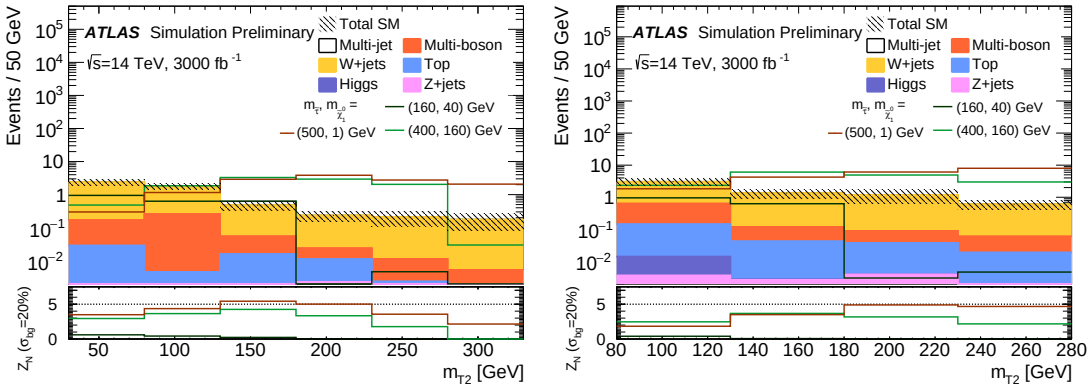

(c) SR-high m_{T2}

(d) SR-exclHigh m_{T2}

Figure 2: Distributions of each m_{T2} variable in the SR-low, SR-med, SR-high and SR-exclHigh regions, applying all selections as specified in Table 2, with the exception of m_{T2} itself. The stacked histograms show the expected SM backgrounds, while the hatched bands represent the statistical uncertainties on the total SM background. For illustration, the distributions of the SUSY reference points for combined $\tilde{\tau}_{\mathrm{L}}^{+}\tilde{\tau}_{\mathrm{L}}^{-}$ and $\tilde{\tau}_{\mathrm{R}}^{+}\tilde{\tau}_{\mathrm{R}}^{-}$ production are also shown as dashed lines. The last bin includes the overflow. The lower pad in each plot shows the significance, Z_N using a background uncertainty of 20%, for the SUSY reference points. In (a), (b) and (c), Z_N is shown for an m_{T2} threshold, while for (d), Z_N is shown in each m_{T2} interval.

by a factor of 0.6 and the tau ID efficiency uncertainty is scaled by a factor of 0.45. The multi-jet uncertainties scale with the increased integrated luminosity, and the background theoretical uncertainties are halved. The theoretical cross-section uncertainty for direct stau production is taken as 10%, while the MC/data related systematics are considered negligible. All other uncertainties are assumed to be the same as the 13 TeV studies. In this Baseline Uncertainties assumption, the total background experimental uncertainty is $\sim$ 19%, with theoretical uncertainties on the Top, Z/γ^* + jets and Higgs backgrounds of 13%, theoretical uncertainties on the W+jets and multi-jet backgrounds of 10%, and uncertainties on the multi-boson background of 8%. The total uncertainty on the SUSY signal is $\sim$ 14%.

A second scenario is also considered, where the expected uncertainties at the HL-LHC do not improve upon the 13 TeV studies for the SM background and signal. This results in a total background uncertainty of $\sim$ 38% and a signal uncertainty of $\sim$ 21% for the Run-2 Uncertainties scenario.

To calculate the discovery potential, SR-low, SR-med and SR-High defined in Table 2 are used, while for the model dependent exclusion limits the best expected signal region is used, considering SR-low, SR-med, SR-High, and the multi-bin SR-exclHigh. Experimental uncertainties are treated as correlated between signal and background and all uncertainties are treated as correlated across regions. The 95% CL exclusion and discovery potentials for combined $\tilde{\tau}_L^+\tilde{\tau}_L^-$ and $\tilde{\tau}_R^+\tilde{\tau}_R^-$ production, $\tilde{\tau}_L^+\tilde{\tau}_L^-$ production alone and $\tilde{\tau}_R^+\tilde{\tau}_R^-$ production alone under different uncertainty assumptions are shown in Figure 3. The $\pm 1\sigma_{\text{exp}}$ uncertainty band indicates the impact on the expected limit of the uncertainty included in the fit. For the Baseline Uncertainties scenario, the exclusion limit reaches 730 GeV in $\tilde{\tau}$ mass for the combined $\tilde{\tau}_L^+\tilde{\tau}_L^-$ and $\tilde{\tau}_R^+\tilde{\tau}_R^-$ production, and 680 GeV (420 GeV) for pure $\tilde{\tau}_L^+\tilde{\tau}_L^-$ (pure $\tilde{\tau}_R^+\tilde{\tau}_R^-$) production with a massless $\tilde{\chi}_1^0$. The discovery sensitivity reaches 110 – 530 GeV (110 – 500 GeV) in $\tilde{\tau}$ mass for the combined $\tilde{\tau}_L^+\tilde{\tau}_L^-$ and $\tilde{\tau}_R^+\tilde{\tau}_R^-$ (pure $\tilde{\tau}_L^+\tilde{\tau}_L^-$) production with a massless $\tilde{\chi}_1^0$. No discovery sensitivity is found for pure $\tilde{\tau}_R^+\tilde{\tau}_R^-$ production as the production cross section is very small.

For the Run-2 Uncertainties scenario, the exclusion limit is slightly reduced to 720 GeV in $\tilde{\tau}$ mass for the combined $\tilde{\tau}_L^+\tilde{\tau}_L^-$ and $\tilde{\tau}_R^+\tilde{\tau}_R^-$ production, and 670 GeV (390 GeV) for pure $\tilde{\tau}_L^+\tilde{\tau}_L^-$ (pure $\tilde{\tau}_R^+\tilde{\tau}_R^-$) production with a massless $\tilde{\chi}_1^0$. The discovery sensitivity is also slightly reduced, reaching 200 – 500 GeV (210 – 460 GeV) in $\tilde{\tau}$ mass for the combined $\tilde{\tau}_L^+\tilde{\tau}_L^-$ and $\tilde{\tau}_R^+\tilde{\tau}_R^-$ (pure $\tilde{\tau}_L^+\tilde{\tau}_L^-$) production with a massless $\tilde{\chi}_1^0$.

Based on the search channels and methods considered here, the HL-LHC is not expected to have discovery potential for the stau co-annhilitation scenario or for the production of light right-handed stau pairs, making these scenarios excellent benchmarks for further study at HL-LHC as well as for future collider-based experiments.

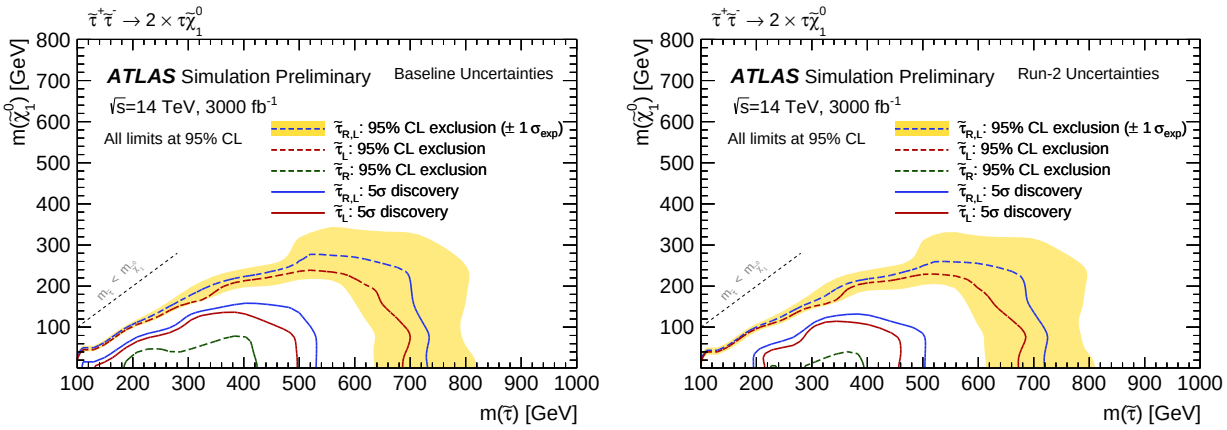

(a) Baseline Uncertainties

(b) Run-2 Uncertainties

Figure 3: The 95% CL exclusion and discovery potential for direct stau production at the HL-LHC (3000fb^{-1} at $\sqrt{s} = 14$ TeV), assuming $\tilde{\tau}_L^+\tilde{\tau}_L^- + \tilde{\tau}_R^+\tilde{\tau}_R^-$ production, $\tilde{\tau}_L^+\tilde{\tau}_L^-$ production, or $\tilde{\tau}_R^+\tilde{\tau}_R^-$ production, for (a) the Baseline Uncertainties scenario and (b) the Run-2 Uncertainties scenario.

5 Search for chargino pair production

In many SUSY models, the charged wino or higgsino states are light and decay via SM gauge bosons [50, 51]. A simplified model describing the direct production of $\tilde{\chi}_1^+\tilde{\chi}_1^-$ is studied here, where the $\tilde{\chi}_1^\pm$ is assumed to be pure wino, while the $\tilde{\chi}_1^0$ is the LSP and is assumed to be pure bino and stable. The $\tilde{\chi}_1^\pm$ decays with 100% branching fraction to $W^\pm$ and $\tilde{\chi}_1^0$, as seen in Figure 4. Only the leptonic decays of the W are considered, resulting in final states with two opposite electric charge (OS) leptons and missing transverse momentum from the two undetected $\tilde{\chi}_1^0$.

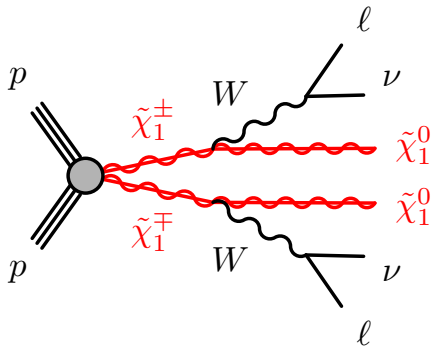

Figure 4: Diagram illustrating the signal scenario considered for the pair production of charginos targeted by the 2ℓ final state.

The selection here closely follows the strategies adopted in the 8 TeV [52] and 13 TeV [53] searches. Events are required to contain exactly two leptons (electrons or muons) with $p_T > 20$ GeV and $|\eta| < 2.5$ (2.47 for electrons). The lepton pair must satisfy $m_{\ell\ell} > 25$ GeV to remove contributions from low mass resonances. The two leptons must be OS, pass "tight" identification criteria [21], and be isolated (the scalar sum of the transverse momenta of charged particles with $p_T > 1$ GeV within a cone of $\Delta R = 0.3$ around the lepton candidate, excluding the lepton candidate track itself, must be less than 15% of the

lepton p_{T}). Jets are defined with $p_{\mathrm{T}} > 30\,\mathrm{GeV}$ and $|\eta| < 2.5$, and a b-tagging algorithm is used on those jets to correctly identify b-quark jets in simulated $t\bar{t}$ samples with an average efficiency of 85%, with a light-flavour jet misidentification probability of a few percent (parametrised as a function of jet p_{T} and η). All leptons are required to be separated from each other and from jets. The latter requirement is imposed to suppress the background from semi-leptonic decays of heavy-flavour quarks, which is further suppressed by vetoing events having one or more b-tagged jets.

The selection strategy is shown in Table 5. The signal region is divided into two disjoint regions with a Same Flavour Opposite Sign (SFOS: e^+e^-, $\mu^+\mu^-$) or Different Flavour Opposite Sign (DFOS: $e^\pm\mu^\mp$) lepton pair to take advantage of the differing SM background composition for each flavour combination. The SFOS and DFOS regions are divided again into events with exactly zero jets or one jet, which target scenarios with large or small $\tilde{\chi}_1^\pm - \tilde{\chi}_1^0$ mass splittings, respectively. One lepton must have $p_{\mathrm{T}} > 40\,\mathrm{GeV}$ to suppress the SM background, and with $p_{\mathrm{T}}^{\ell 1} > 40\,\mathrm{GeV}$ and $p_{\mathrm{T}}^{\ell 2} > 20\,\mathrm{GeV}$, either the single or double lepton triggers may be used to accept the event at the HL-LHC. Events with SFOS lepton pairs with an invariant mass within 30 GeV of the Z boson mass are rejected to suppress the large $Z \to \ell\ell$ SM background. Large $E_{\mathrm{T}}^{\mathrm{miss}}$ and $E_{\mathrm{T}}^{\mathrm{miss}}$ significance ($E_{\mathrm{T}}^{\mathrm{miss}}$ significance $= E_{\mathrm{T}}^{\mathrm{miss}}/\sqrt{\sum p_{\mathrm{T}}^{\text{leptons, jets}}}$) are chosen in accordance with the 13 TeV analysis [53] to suppress Z+jets events with poorly measured leptons.

The stransverse mass m_{T2} defined in Equation 1 is calculated using the two leptons and $E_{\mathrm{T}}^{\mathrm{miss}}$, and used as the main discriminator in the SR selection to suppress the SM background. For $t\bar{t}$ or WW decays, assuming an ideal detector with perfect momentum resolution, $m_{\mathrm{T2}}(\ell, \ell, E_{\mathrm{T}}^{\mathrm{miss}})$ has a kinematic endpoint at the mass of the W boson. Signal models with sufficient mass splittings between the $\tilde{\chi}_1^\pm$ and the $\tilde{\chi}_1^0$ feature m_{T2} distributions that extend beyond this kinematic endpoint expected for the dominant SM backgrounds. Therefore, events in this search are required to have high m_{T2} values. A set of disjoint signal regions "binned" in m_{T2} are used to maximise model-dependent exclusion sensitivity. Each SR is identified by the lepton flavour combination (SFOS or DFOS), number of jets (-0J or -1J) and the range of the m_{T2} interval, as seen in Table 5.

The stransverse mass m_{T2} of SM and SUSY events in the signal regions is shown in Figure 5, for events passing $m_{\mathrm{T2}} > 100\,\mathrm{GeV}$. Generally, the SM backgrounds drop off at lower m_{T2} values (around the W mass), while the SUSY signal and 2ℓ diboson processes are seen to have long tails to high m_{T2} values. In the 13 TeV analysis [53], long tails in m_{T2} for 2ℓ diboson processes were seen to be from the imperfect measurement of the leptons and $E_{\mathrm{T}}^{\mathrm{miss}}$ in WW, as well as $ZZ \to \ell^+\ell^-\nu\bar{\nu}$. Eleven high m_{T2} intervals are defined to maximise the sensitivity to $\tilde{\chi}_1^+\tilde{\chi}_1^-$ production and the expected number of events from SM and SUSY processes in these signal regions are shown in Figure 5. After the application of the Z veto, lepton p_{T} thresholds and high m_{T2}, no Z+jets or W+jets events remain. The diboson processes are seen to dominate the total SM background across all signal regions. In the 13 TeV analysis this was seen to be mostly WW, due to its similarity with the SUSY signal.

To calculate the expected sensitivity to $\tilde{\chi}_1^+\tilde{\chi}_1^-$ production and decay via W bosons, the expected uncertainties on the SM background are assessed. The level of accuracy achieved ($7 - 17\%$) in the 13 TeV analysis [53] was dominated by the normalisation of the WW background (5%) and theoretical uncertainties on the WW background ($\sim 5 - 10\%$), while the experimental uncertainties were $\sim 5\%$. The $t\bar{t}$ normalisation and theoretical uncertainties were similar to those for the WW background. It is expected that the uncertainties from the normalisation of the WW background will scale inversely with the increase in luminosity, and thus decrease to $\sim 1\%$, while a better understanding of WW could halve the theoretical uncertainties to $\sim 2.5 - 5\%$. It is assumed that the experimental uncertainties will be understood to the same level, or better, than the 13 TeV analysis. Two scenarios for the uncertainties are considered for $\tilde{\chi}_1^+\tilde{\chi}_1^-$

Table 5: Signal regions for the direct chargino pair production analysis.

	Common			
$m_{\ell\ell}$ > [GeV]	25			
$p_{\mathrm{T}}^{\mathrm{lep1}}, p_{\mathrm{T}}^{\mathrm{lep2}}$ > [GeV]	40, 20			
number of b jets	= 0			
$E_{\mathrm{T}}^{\mathrm{miss}}$ > [GeV]	110			
$E_{\mathrm{T}}^{\mathrm{miss}}$ sig > [GeV$^{1/2}$]	10			
	SR-SFOS-0J	SR-SFOS-1J	SR-DFOS-0J	SR-DFOS-1J
lepton flavour/sign	SFOS		DFOS	
$\lvert m_{\mathrm{SFOS}} - m_Z \rvert$ > [GeV]	30		–	
number of jets	= 0	= 1	= 0	= 1
m_{T2} [GeV]	∈ [100, 120]			
	∈ [120, 140]			
	∈ [140, 140]			
	∈ [160, 180]			
	∈ [180, 200]			
	∈ [200, 250]			
	∈ [250, 300]			
	∈ [300, 350]			
	∈ [350, 400]			
	∈ [400, 500]			
	∈ [500, ∞]			

production and decay via W bosons at the HL-LHC, both assuming a 5% experimental uncertainty on the signal and SM background, and a 10% theoretical uncertainty on the signal. For the Run-2 Uncertainties scenario, the modelling uncertainty on the SM background is assumed to remain the same as for Run-2, at 10%. For the Baseline Uncertainties scenario, it is assumed the modelling of the WW background can be understood to a better level, and the modelling uncertainty on the SM background halves to just 5%.

The statistical combination of all disjoint signal regions is used to set model-dependent exclusion limits. For each of the three uncertainties considered, half of the value is treated as correlated across signal regions, and the other half as uncorrelated. The exclusion potentials for $\tilde{\chi}_1^+\tilde{\chi}_1^-$ production and decay via W bosons at the HL-LHC are shown in Figure 6. For the Run-2 Uncertainties scenario in the absence of an excess, $\tilde{\chi}_1^+\tilde{\chi}_1^-$ production may be excluded up to 840 GeV in $\tilde{\chi}_1^\pm$ mass. For the Baseline Uncertainties scenario, where the modelling uncertainty on the SM background halves from 10% to 5%, the expected exclusion potential increases by just a few GeV in $\tilde{\chi}_1^\pm$ mass and 20 GeV in $\tilde{\chi}_1^0$ mass. To calculate the discovery potential, eleven inclusive signal regions are defined with m_{T2} larger than the lower bound of each m_{T2} interval in Table 5, and the inclusive signal region with the best expected sensitivity is used. At the HL-LHC, the discovery potential reaches up to 610 GeV in $\tilde{\chi}_1^\pm$ mass for the Run-2 Uncertainties scenario, as seen in Figure 6(b). For the Baseline Uncertainties scenario, the discovery potential is extended by a further 50 GeV in $\tilde{\chi}_1^\pm$ mass and 80 GeV in $\tilde{\chi}_1^0$ mass.

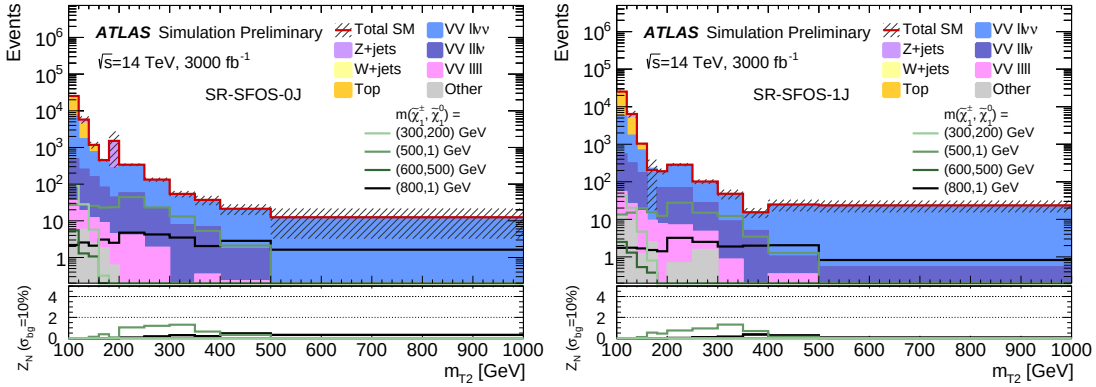

(a) SR-SFOS-0J

(b) SR-SFOS-1J

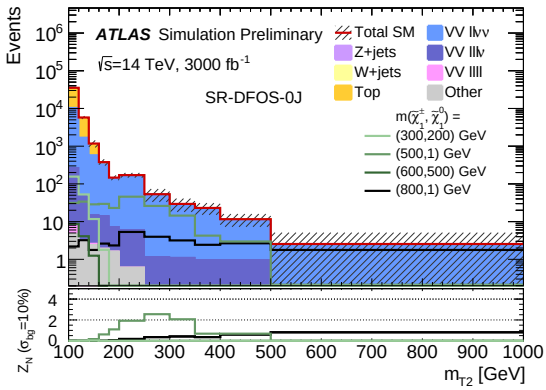

(c) SR-DFOS-0J

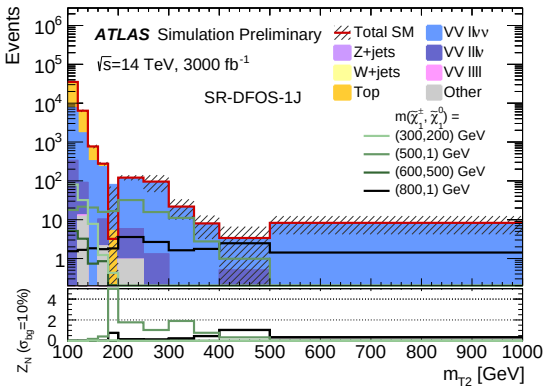

(d) SR-DFOS-1J

Figure 5: The expected number of events from SM and SUSY processes in the signal regions optimised for $\tilde{\chi}_1^+\tilde{\chi}_1^-$ production, for the HL-LHC. Uncertainties shown are the MC statistical uncertainties only. "Top" is the sum of the $t\bar{t}$ and single top backgrounds, while "Other" is the sum of the $t\bar{t}W$ and $t\bar{t}WW$ backgrounds. The last bin includes the overflow. The lower pad in each plot shows the significance, Z_N using a background uncertainty of 10%, for a selection of SUSY scenarios in each m_{T2} interval.

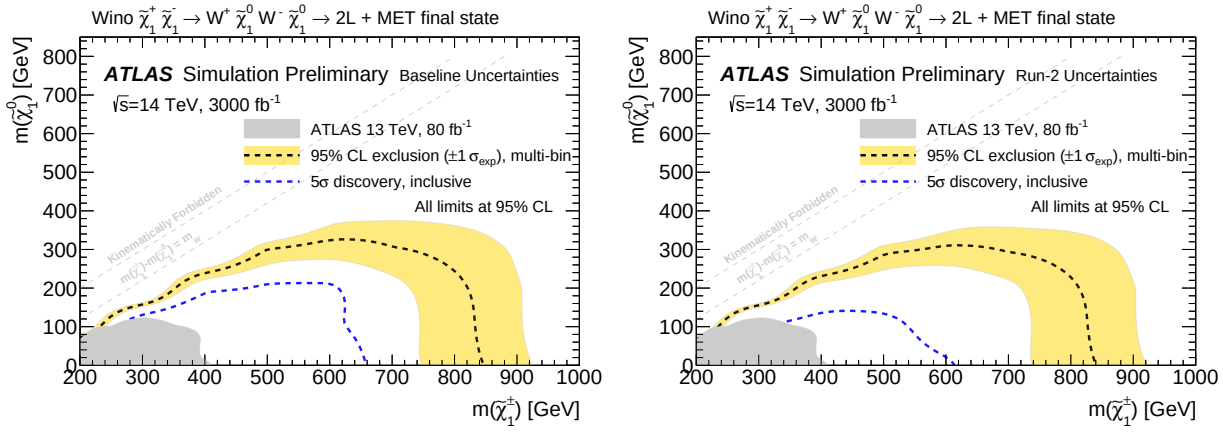

(a) Baseline Uncertainties, $\sigma_{\text{bg}}^{\text{modelling}} = 5\%$

(b) Run-2 Uncertainties, $\sigma_{\text{bg}}^{\text{modelling}} = 10\%$

Figure 6: The 95% CL exclusion and discovery potential for $\tilde{\chi}_1^+ \tilde{\chi}_1^-$ production at the HL-LHC (3000fb^{-1} at $\sqrt{s} = 14$ TeV), assuming $\tilde{\chi}_1^\pm \rightarrow W \tilde{\chi}_1^0$ with a branching ratio of 100%, for an uncertainty on the modelling of the SM background of (a) 5% or (b) 10%. The observed limits from the analyses of 13 TeV data [53] are also shown.

6 Search for chargino-neutralino pair production

A simplified model describing the direct production of $\tilde{\chi}_1^\pm \tilde{\chi}_2^0$ is studied here, where the $\tilde{\chi}_1^\pm$ and $\tilde{\chi}_2^0$ are assumed to be pure wino and equal mass, while the $\tilde{\chi}_1^0$ is the LSP and is assumed to be pure bino and stable. The $\tilde{\chi}_1^\pm$ is assumed to decay with 100% branching fraction to $W^\pm$ and $\tilde{\chi}_1^0$, while two scenarios are considered for the $\tilde{\chi}_2^0$ decay, $\tilde{\chi}_2^0 \to Z\tilde{\chi}_1^0$ with 100% branching fraction as seen in Figure 7(a) or $\tilde{\chi}_2^0 \to h\tilde{\chi}_1^0$ with 100% branching fraction as seen in Figure 7(b). For $\tilde{\chi}_2^0 \to h\tilde{\chi}_1^0$, the light CP-even Higgs boson, h, of the MSSM Higgs sector is assumed to be practically identical to the SM Higgs boson [54], with the same mass and couplings as measured at the LHC [55–57]. A search for $\tilde{\chi}_1^\pm \tilde{\chi}_2^0 \to W\tilde{\chi}_1^0 Z\tilde{\chi}_1^0$ using the three lepton (e, μ) final state is described in Section 6.1, while the $1\ell bb$ final state is used for $\tilde{\chi}_1^\pm \tilde{\chi}_2^0 \to W\tilde{\chi}_1^0 h\tilde{\chi}_1^0$ and is described in Section 6.2.

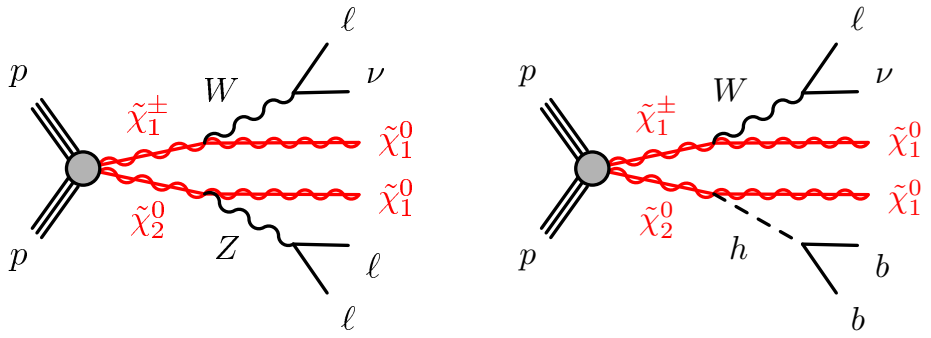

(a) (b)

Figure 7: Diagrams illustrating the signal scenarios considered for the pair production of chargino and next-to-lightest neutralino which subsequently decay via (a) a Z boson or (b) a Higgs boson h, targeted by the 3ℓ and $1\ell b\bar{b}$ final states respectively.

6.1 Search for $\tilde{\chi}_1^\pm \tilde{\chi}_2^0 \to W\tilde{\chi}_1^0 Z\tilde{\chi}_1^0$ using three leptons

The selection for $\tilde{\chi}_1^\pm \tilde{\chi}_2^0 \to W\tilde{\chi}_1^0 Z\tilde{\chi}_1^0$ at the HL-LHC follows the strategy used in the 13 TeV search [58]. Events are selected with exactly three leptons (electrons or muons) with $p_\mathrm{T} > 20$ GeV and $|\eta| < 2.5$, two of which must form an SFOS pair consistent with a Z boson decay and have $|m_{\ell\ell} - m_Z| < 10$ GeV. To resolve ambiguities when multiple SFOS pairings are present, the transverse mass m_T is calculated using the unpaired lepton for each possible SFOS pairing, and the combination that minimises the transverse mass, $m_\mathrm{T}^\mathrm{min}$, is chosen. The two leading leptons must have $p_\mathrm{T} > 25$ GeV, and $m_{\ell\ell\ell}$ must be larger than 20 GeV to reject low mass SM decays. To suppress the $t\bar{t}$ background, events are vetoed if they contain b-tagged jets with $p_\mathrm{T} > 30$ GeV and $|\eta| < 2.5$, while the Z+jets background is suppressed by requiring $E_\mathrm{T}^\mathrm{miss} > 50$ GeV. The chosen working point of the b-tagging algorithm correctly identifies b-quark jets in simulated $t\bar{t}$ samples with an average efficiency of 77%.

A set of disjoint signal regions binned in $m_\mathrm{T}^\mathrm{min}$ and $E_\mathrm{T}^\mathrm{miss}$ are used to maximise model-dependent exclusion sensitivity. Each SR is identified by the number of jets with $p_\mathrm{T} > 30$ GeV and $|\eta| < 2.5$ (-0J or -1J), the range of the $E_\mathrm{T}^\mathrm{miss}$ interval and the range of the $m_\mathrm{T}^\mathrm{min}$ interval, as seen in Table 6.1. The SRs with at least one jet target signal scenarios in which the mass differences between the $\tilde{\chi}_1^+$ and $\tilde{\chi}_1^0$ is small. In such scenarios

higher $E_{\mathrm{T}}^{\mathrm{miss}}$ in the event is expected when the $\tilde{\chi}_1^{\pm}\tilde{\chi}_2^0$ system recoils against the initial-state-radiation (ISR) jets. The distributions of $E_{\mathrm{T}}^{\mathrm{miss}}$ and $m_{\mathrm{T}}^{\mathrm{min}}$ in the 0-jet and 1-jet categories are shown in Figure 8 for events with $E_{\mathrm{T}}^{\mathrm{miss}} > 150\,\mathrm{GeV}$ and $m_{\mathrm{T}}^{\mathrm{min}} > 150\,\mathrm{GeV}$.

Table 6: Signal regions for the search for chargino-neutralino pair production and decay to three leptons.

Common						
lepton flavour/sign	$e^+e^-\ell^\pm$ or $\mu^+\mu^-\ell^\pm$					
$p_{\mathrm{T}}^{\ell 1}, p_{\mathrm{T}}^{\ell 2}, p_{\mathrm{T}}^{\ell 3} >$ [GeV]	25, 25, 20					
$\lvert m_{\mathrm{SFOS}} - m_Z\rvert <$ [GeV]	10					
$m_{\ell\ell\ell} >$ [GeV]	20					
number of b jets	= 0					
SR	SR-0J		SR-1J		Inclusive	
number of jets	= 0		≥ 1		≥ 0	
[GeV]	$m_{\mathrm{T}}^{\mathrm{min}}$	$E_{\mathrm{T}}^{\mathrm{miss}}$	$m_{\mathrm{T}}^{\mathrm{min}}$	$E_{\mathrm{T}}^{\mathrm{miss}}$	$m_{\mathrm{T}}^{\mathrm{min}}$	$E_{\mathrm{T}}^{\mathrm{miss}}$
	∈ [150, 250]	∈ [200, 250]	∈ [150, 250]	∈ [200, 250]	> 250	> 200
		∈ [250, 350]		∈ [250, 350]		> 250
		∈ [350, 450]		∈ [350, 450]		> 350
		∈ [450, ∞]		∈ [450, 600]		> 450
				∈ [600, ∞]		> 500
						> 600
	∈ [250, 400]	∈ [150, 250]	∈ [250, 400]	∈ [150, 250]	> 400	> 200
		∈ [250, 350]		∈ [250, 350]		> 250
		∈ [350, 500]		∈ [350, 500]		> 350
		∈ [500, ∞]		∈ [500, ∞]		> 450
						> 500
						> 600
	∈ [400, ∞]	∈ [150, 350]	∈ [400, ∞]	∈ [150, 350]		
		∈ [350, 450]		∈ [350, 450]		
		∈ [450, 600]		∈ [450, 600]		
		∈ [600, ∞]		∈ [600, ∞]		

The expected number of events in the exclusive SRs, SR-0J and SR-1J, are summarised in Tables 7 and 8. In all regions the dominant background is WZ production (80 – 100% of the total background), followed by the fakes from $t\bar{t}$ and $t\bar{t}V/\gamma$.

The exclusive SRs in the 13 TeV analysis [58] were dominated by statistical uncertainties on the background estimation (5 – 30%), while uncertainties on the diboson modelling (1 – 6%) and those on jet and $E_{\mathrm{T}}^{\mathrm{miss}}$ modelling (2 – 7%) were also important. It is expected that the statistical uncertainties on the background estimation will scale with the inverse of the square root of the luminosity, and decrease to 1 – 5%. It is assumed that the experimental uncertainties will be understood to the same level as the 13 TeV analysis.

The statistical combination of all disjoint signal regions is used to set model-dependent exclusion limits. The expected sensitivity to $(\tilde{\chi}_1^{\pm}/\tilde{\chi}_2^0)$ production is calculated considering 5% experimental uncertainties on the SM background and signal, a 10% theoretical uncertainty on the signal, and a 10% modelling uncertainty on the SM. For each of the three uncertainties considered, half of the value is treated as correlated across signal regions, and the other half as uncorrelated. With this Baseline Uncertainties scenario, Figure 9 shows the expected exclusion for $\tilde{\chi}_1^{\pm}\tilde{\chi}_2^0 \to W\tilde{\chi}_1^0 Z\tilde{\chi}_1^0$. In the absence of an excess,

Table 7: The expected number of events from SM and SUSY processes in the three lepton 0J signal regions optimised for $\tilde{\chi}_1^{\pm}\tilde{\chi}_2^0 \to W\tilde{\chi}_1^0 Z\tilde{\chi}_1^0$ at the HL-LHC. Uncertainties shown describe the MC statistical uncertainties only. The event yields for two signal scenarios are also shown.

$m_{\mathrm{T}}^{\mathrm{min}} \in [150, 250]$ GeV $E_{\mathrm{T}}^{\mathrm{miss}}$ [GeV]	[200,250]	[250,350]	[350,450]	> 450
Total SM	190 ± 10	42 ± 6	5 ± 1	1.4 ± 0.7
$m(\tilde{\chi}_1^{\pm}/\tilde{\chi}_2^0, \tilde{\chi}_1^0) = (1100, 0)$ GeV	0.11 ± 0.03	0.44 ± 0.07	0.26 ± 0.05	0.88 ± 0.09
$m(\tilde{\chi}_1^{\pm}/\tilde{\chi}_2^0, \tilde{\chi}_1^0) = (600, 400)$ GeV	13 ± 2	11 ± 2	2.6 ± 0.8	1.2 ± 0.5
$m_{\mathrm{T}}^{\mathrm{min}} \in [250, 400]$ GeV $E_{\mathrm{T}}^{\mathrm{miss}}$ [GeV]	[150,250]	[250,350]	[350,450]	> 450
Total SM	34 ± 3	10 ± 5	4.1 ± 1.2	1.1 ± 0.7
$m(\tilde{\chi}_1^{\pm}/\tilde{\chi}_2^0, \tilde{\chi}_1^0) = (1100, 0)$ GeV	0.1 ± 0.03	0.36 ± 0.06	0.56 ± 0.07	1.4 ± 0.1
$m(\tilde{\chi}_1^{\pm}/\tilde{\chi}_2^0, \tilde{\chi}_1^0) = (600, 400)$ GeV	11 ± 1	8 ± 1	2.6 ± 0.8	0 ± 0
$m_{\mathrm{T}}^{\mathrm{min}} > 400$ GeV $E_{\mathrm{T}}^{\mathrm{miss}}$ [GeV]	[150,350]	[350,450]	[450,600]	> 600
Total SM	35 ± 3	8 ± 2	6 ± 1	2.1 ± 0.8
$m(\tilde{\chi}_1^{\pm}/\tilde{\chi}_2^0, \tilde{\chi}_1^0) = (1100, 0)$ GeV	0.41 ± 0.06	0.73 ± 0.09	1.3 ± 0.1	3.6 ± 0.2
$m(\tilde{\chi}_1^{\pm}/\tilde{\chi}_2^0, \tilde{\chi}_1^0) = (600, 400)$ GeV	4.2 ± 0.9	1.2 ± 0.5	0.23 ± 0.23	0 ± 0

Table 8: The expected number of events from SM and SUSY processes in the three lepton 1J signal regions optimised for $\tilde{\chi}_1^{\pm}\tilde{\chi}_2^0 \to W\tilde{\chi}_1^0 Z\tilde{\chi}_1^0$ at the HL-LHC. Uncertainties shown describe the MC statistical uncertainties only. The event yields for two signal scenarios are also shown.

$m_{\mathrm{T}}^{\mathrm{min}} \in [150, 250]$ GeV $E_{\mathrm{T}}^{\mathrm{miss}}$ [GeV]	[200,250]	[250,350]	[350,450]	[450,600]	> 600
Total SM	220 ± 15	74 ± 7	11 ± 2	6.2 ± 1.3	1.6 ± 0.9
$m(\tilde{\chi}_1^{\pm}/\tilde{\chi}_2^0, \tilde{\chi}_1^0) = (1100, 0)$ GeV	0.11 ± 0.03	0.38 ± 0.06	0.33 ± 0.06	0.48 ± 0.07	0.43 ± 0.07
$m(\tilde{\chi}_1^{\pm}/\tilde{\chi}_2^0, \tilde{\chi}_1^0) = (600, 400)$ GeV	9.4 ± 1.1	14 ± 2	4.2 ± 1.1	2.8 ± 0.8	1.4 ± 0.6
$m_{\mathrm{T}}^{\mathrm{min}} \in [250, 400]$ GeV $E_{\mathrm{T}}^{\mathrm{miss}}$ [GeV]	[150,250]	[250,350]	[350,500]	> 500	
Total SM	46 ± 8	21 ± 9	9.3 ± 2.4	2.5 ± 0.9	
$m(\tilde{\chi}_1^{\pm}/\tilde{\chi}_2^0, \tilde{\chi}_1^0) = (1100, 0)$ GeV	0.09 ± 0.03	0.36 ± 0.06	0.72 ± 0.09	1.2 ± 0.1	
$m(\tilde{\chi}_1^{\pm}/\tilde{\chi}_2^0, \tilde{\chi}_1^0) = (600, 400)$ GeV	7.3 ± 1.2	10 ± 1	4.2 ± 1.2	2.1 ± 0.7	
$m_{\mathrm{T}}^{\mathrm{min}} > 400$ GeV $E_{\mathrm{T}}^{\mathrm{miss}}$ [GeV]	[150,350]	[350,450]	[450,600]	> 600	
Total SM	31 ± 3	6.2 ± 1.4	4.3 ± 1.1	1.3 ± 0.7	
$m(\tilde{\chi}_1^{\pm}/\tilde{\chi}_2^0, \tilde{\chi}_1^0) = (1100, 0)$ GeV	0.44 ± 0.07	0.64 ± 0.08	1.3 ± 0.1	3.6 ± 0.2	
$m(\tilde{\chi}_1^{\pm}/\tilde{\chi}_2^0, \tilde{\chi}_1^0) = (600, 400)$ GeV	3.7 ± 0.9	1.4 ± 0.6	0.47 ± 0.33	0.47 ± 0.33	

chargino and neutralino masses up to 1150 GeV may be excluded. The discovery potential is also shown in Figure 9, which reaches up to 920 GeV in chargino and neutralino masses. To calculate the discovery potential, twelve inclusive signal regions with $n_{\mathrm{jets}} > 0$ and lower thresholds on $E_{\mathrm{T}}^{\mathrm{miss}}$ and $m_{\mathrm{T}}^{\mathrm{min}}$ are defined,

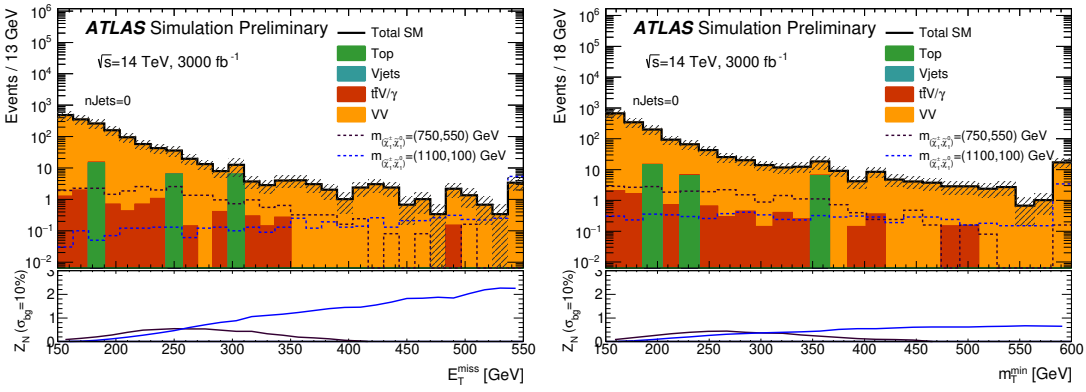

(a) $E_{\mathrm{T}}^{\mathrm{miss}}$, 0J (b) $m_{\mathrm{T}}^{\mathrm{min}}$, 0J

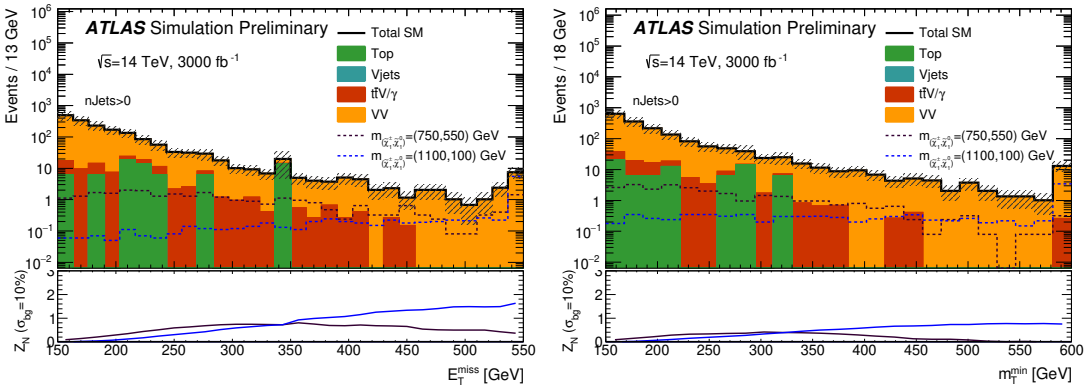

(c) $E_{\mathrm{T}}^{\mathrm{miss}}$, 1J (d) $m_{\mathrm{T}}^{\mathrm{min}}$, 1J

Figure 8: The distribution of $E_{\mathrm{T}}^{\mathrm{miss}}$ and $m_{\mathrm{T}}^{\mathrm{min}}$ in the events with zero jets (top) and the events with at least one jet (bottom). All common requirements along with $E_{\mathrm{T}}^{\mathrm{miss}} > 150\,\mathrm{GeV}$ and $m_{\mathrm{T}}^{\mathrm{min}} > 150\,\mathrm{GeV}$ are applied. The last bin includes the overflow. The lower pad in each plot shows the significance for the SUSY reference points, Z_N, as the threshold on the x-axis variable increases and assumes a background uncertainty of 10%.

as shown in Table . The inclusive search region which gives the best expected sensitivity is used for the discovery potential calculation.

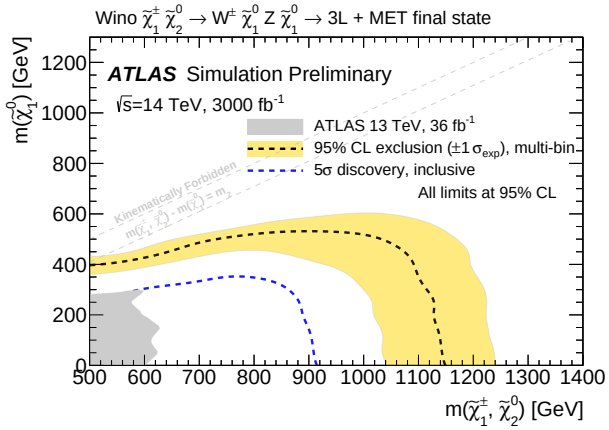

Figure 9: The 95% CL exclusion and discovery potential for $\tilde{\chi}_1^\pm \tilde{\chi}_2^0$ production at the HL-LHC (3000fb^{-1} at $\sqrt{s} = 14$ TeV), assuming $\tilde{\chi}_1^\pm \to W\tilde{\chi}_1^0$ and $\tilde{\chi}_2^0 \to Z\tilde{\chi}_1^0$ with a branching ratio of 100%. The observed limits from the analyses of 13 TeV data [52, 58–60] are also shown.

6.2 Search for $\tilde{\chi}_1^\pm \tilde{\chi}_2^0 \to W\tilde{\chi}_1^0 h\tilde{\chi}_1^0$ using $1\ell bb$

This analysis updates the previous studies in the same final states for the HL-LHC as in Ref. [61], using the latest parameterisations of the upgraded ATLAS detector configurations for the $\langle\mu\rangle \sim 200$ HL-LHC running conditions and the associated physics object systematic uncertainties, as well as a re-optimised multivariate based analysis method.

Signal models with $\tilde{\chi}_1^\pm$ and $\tilde{\chi}_2^0$ masses up to 1500 GeV are considered. The analysis is performed separately in three signal regions targetting signal models with different values of mass difference $\Delta m = m(\tilde{\chi}_1^\pm/\tilde{\chi}_2^0) - m(\tilde{\chi}_1^0)$, which leads to different kinematic shapes. In each region, one benchmark signal model is selected as a reference point for the optimisation of event selections and sensitivity estimations. The definitions of three regions and the corresponding benchmark signal models are:

- Low: $\Delta m < 300$ GeV, benchmark signal model $m(\tilde{\chi}_1^\pm/\tilde{\chi}_2^0, \tilde{\chi}_1^0) = (500, 310)$ GeV,
- Medium: $\Delta m \in [300, 600]$ GeV, benchmark signal model $m(\tilde{\chi}_1^\pm/\tilde{\chi}_2^0, \tilde{\chi}_1^0) = (800, 420)$ GeV,
- High: $\Delta m > 600$ GeV, benchmark signal model $m(\tilde{\chi}_1^\pm/\tilde{\chi}_2^0, \tilde{\chi}_1^0) = (1000, 1)$ GeV.

At each point in the signal model parameter space, the region with the best sensitivity is chosen for the estimate of the final analysis sensitivities, instead of a statistical combination of the regions. For this reason, event selections in different regions are not necessarily orthogonal.

The expected SM background is dominated by top quark pair-production $t\bar{t}$ and single top production, with smaller contributions from vector boson production W+jets, associated production of $t\bar{t}$ and a vector boson ($t\bar{t}V$) and dibosons.

6.2.1 Event selection

The event selection follows a similar strategy as in the previous studies documented in Ref. [61]. Candidate leptons (electrons or muons) are required to have $p_{\mathrm{T}} > 25$ GeV and $|\eta| < 2.47$ ($|\eta| < 2.7$ for muons), and

pass "tight" and "medium" identification criteria for electrons and muons respectively. Candidate jets are reconstructed using the anti-k_t algorithm with $R = 0.4$, are required to have $p_{\mathrm{T}} > 25\,\mathrm{GeV}$ and $|\eta| < 2.5$. B-tagged jets are required to pass the jet requirements described previously, and pass the MV2c10 tagging algorithm operating at 77% b-jet tagging efficiency. Candidate jets and electrons are required to satisfy $\Delta R(e, \mathrm{jet}) > 0.2$. Any leptons within $\Delta R = 0.4$ of the remaining jet are removed. The $E_{\mathrm{T}}^{\mathrm{miss}}$ at generator level is calculated as the vectorial sum of the momenta of neutral weakly-interacting particles, in this case neutrinos and neutralinos. The detector response is simulated using a set of parametrised functions as described in Section 3.

The impact of the trigger is not taken into account in this analysis. The planned upgrades to the detector, in particular an improved barrel muon coverage, are expected to allow lepton triggers that would have high efficiency for the studied scenarios with respect to the analysis selections.

Events containing exactly one lepton, and two or three jets passing the above object definitions are selected. Exactly two of the jets are required to be b-tagged with the criteria defined above. Four key variables are further used to discriminate signal from background:

- m_{bb} - the invariant mass of the two b-tagged jets
- $E_{\mathrm{T}}^{\mathrm{miss}}$ - the transverse momentum imbalance in the event
- m_{T} - the transverse mass constructed using the lepton p_{T} and the $E_{\mathrm{T}}^{\mathrm{miss}}$.
- m_{CT} - the contransverse mass, defined for the $b\bar{b}$ system as:

$$m_{\mathrm{CT}} = 2p_{\mathrm{T}}^{b_1} p_{\mathrm{T}}^{b_2} (1 + \cos\Delta\phi_{bb}), \tag{2}$$

  where $p_{\mathrm{T}}^{b_1}$ and $p_{\mathrm{T}}^{b_2}$ are transverse momenta of the two leading $b-$jets and $\Delta\phi_{bb}$ is the azimuthal angle between them.

The m_{bb} is used to select events which have dijet masses within a window of the Higgs boson mass. The transverse mass variable m_{T} is effective at suppressing SM backgrounds containing W bosons due to the expected kinematic endpoint around the W boson mass assuming an ideal detector with perfect momentum resolution. The contransverse mass variable m_{CT} is an effective variable to select Higgs boson decays into $b-$quarks and to suppress the $t\bar{t}$ backgrounds [62, 63].

A set of common loose requirements, referred to as preselection, are applied first to suppress the fully hadronic multijet and W+jets backgrounds: $m_{\mathrm{T}} > 40\,\mathrm{GeV}$, $m_{\mathrm{bb}} > 50\,\mathrm{GeV}$, $E_{\mathrm{T}}^{\mathrm{miss}} > 200\,\mathrm{GeV}$. Figure 10 shows the distributions of the key discriminating variables after this selection, comparing the three benchmark signal models with the expected SM background.

To further distinguish between signal and background processes, a set of rectangular selections based on these kinematic observables is first studied to evaluate possible optimal selections and residual SM background. A multivariate method based on boosted decision trees (BDT) is then chosen for the optimal sensitivity. In this approach, three independent BDTs (referred to as M1, M2 and M3), are trained separately in each signal region for events passing the preselection and within the m_{bb} mass window of $[105, 135]\,\mathrm{GeV}$. All the signal MC samples within a given signal region are combined to mimic the average kinematic shapes of the signal. Only the dominant $t\bar{t}$ background is considered in the training. In all regions, the following seven variables are used as inputs: $E_{\mathrm{T}}^{\mathrm{miss}}$, m_{T}, m_{CT}, the lepton p_{T}, the leading and sub-leading b-jet p_{T}, as well as the angular separation of the two b-tagged jets $\Delta R(b_1, b_2)$.

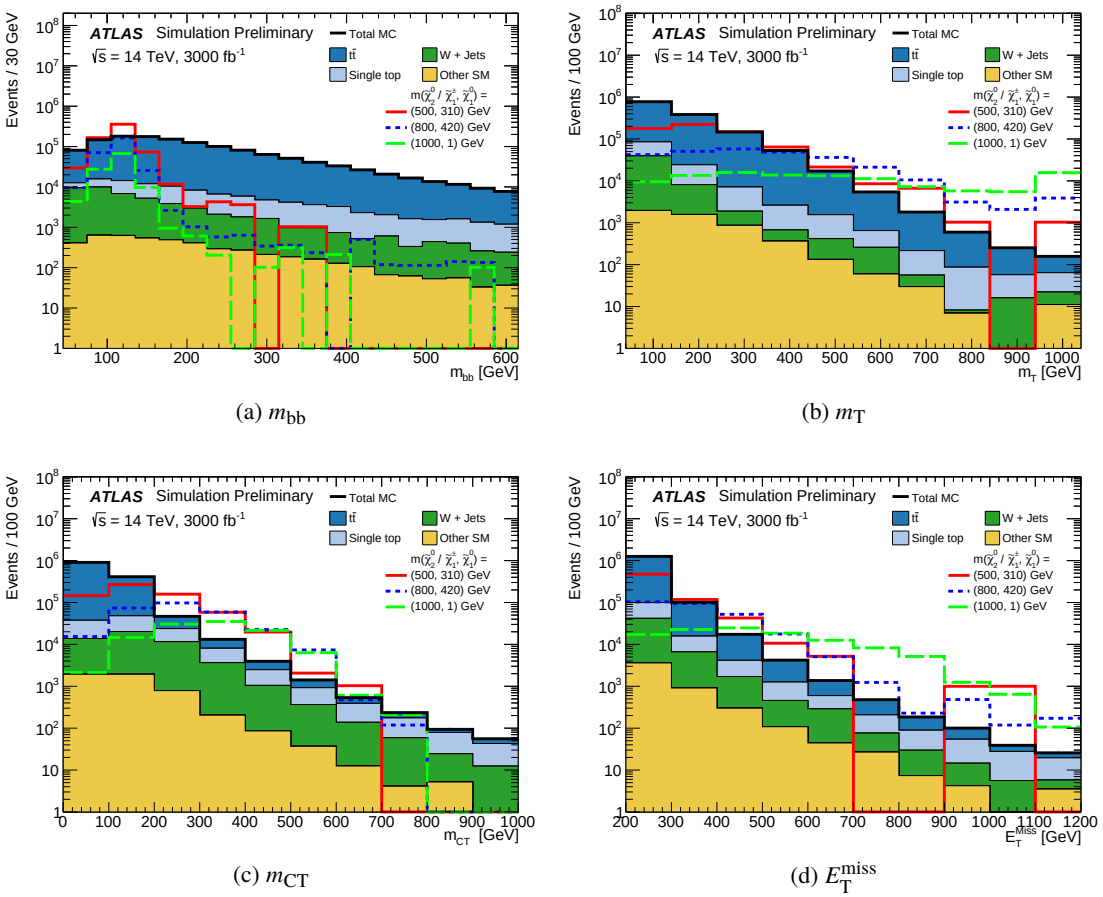

(a) m_{bb} (b) m_{T}

(c) m_{CT} (d) $E_{\mathrm{T}}^{\mathrm{miss}}$

Figure 10: Distributions of the key discriminating variables at the preselection level. The contributions from all SM background are shown as stacked, and the expected distribution from the benchmark signal models are overlaid. The last bin does not include the overflow.

The BDT output distributions are then used to optimise signal regions maximising the expected significance Z_N of the benchmark signal model. Examples of the BDT output distributions are shown in Figure 11. The resulting signal region definitions are shown in Table 9.

Table 9: Definitions of the signal regions with the benchmark signal model parameters used in the optimisation.

SR	Benchmark signal model parameters $m(\tilde{\chi}_1^{\pm}/\tilde{\chi}_2^0, \tilde{\chi}_1^0)$ [GeV]	BDT range
SR-M1	(500, 310)	> 0.25
SR-M2	(800, 420)	> 0.35
SR-M3	(1000, 1)	> 0.30

Table 10 shows the expected number of events for the SM background and three benchmark SUSY scenarios respectively. The SM background is dominated by the top backgrounds, including both the $t\bar{t}$ and single top processes.

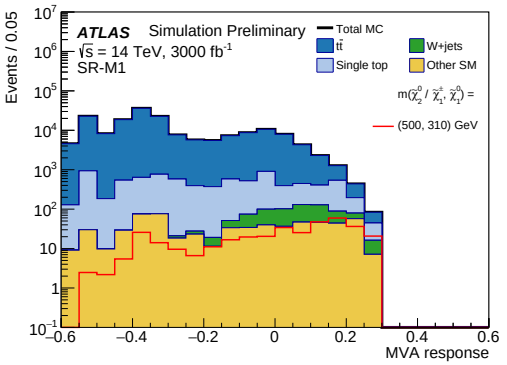

(a) M1

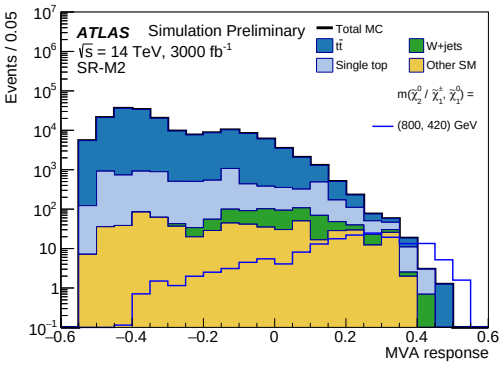

(b) M2

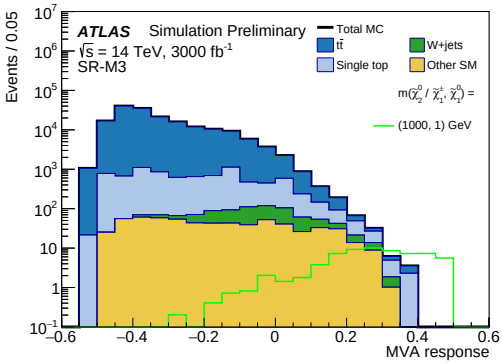

(c) M3

Figure 11: Distributions of the BDT responses in the three signal regions for the events that pass the preselection and are within m_{bb} mass window of [105, 135] GeV. The contributions from all SM background are shown as stacked, and the expected distribution from the benchmark signal models are overlaid.

The largest systematic uncertainties are from theoretical modelling of the irreducible backgrounds of $t\bar{t}$ and single top, mainly from the generator difference, renormalisation and factorisation scale variations and the interference between the $t\bar{t}$ and single top background. The total theoretical uncertainty is estimated to be about 7%. Experimental uncertainties are dominated by the jet energy scale (JES) and jet energy resolution (JER), on the order of 6%.

Figure 12 shows the expected 95% CL exclusion and 5σ discovery contours for the simplified models described earlier. In this model, masses of $\tilde{\chi}_1^{\pm}/\tilde{\chi}_2^0$ up to 1280 GeV could be excluded at 95% confidence level for a massless $\tilde{\chi}_1^0$. The discovery potential at 5σ could be extended up to 1080 GeV for a massless $\tilde{\chi}_1^0$. More mature analysis and reconstruction techniques such as performing a multi-bin shape fit, improving the training in the multivariate method by including other SM backgrounds, using jet substructure techniques in the boosted Higgs boson region, and performing a statistical combination of all signal regions would likely extend the sensitivity even further.

Table 10: Expected number of events for the SM background and the benchmark signal models in the $1\ell bb$ signal regions SR-M1, SR-M2, and SR-M3. The uncertainties describe the MC statistical uncertainties only.

Processes	SR-M1	SR-M2	SR-M3
$t\bar{t}$	38.9 ± 8.4	8.7 ± 3.3	2.5 ± 1.8
single top	28.3 ± 4.8	10.7 ± 3.2	5.4 ± 2.5
W+jets	22.2 ± 5.4	3.0 ± 2.0	2.0 ± 1.8
ttV	5.1 ± 2.4	2.0 ± 1.4	1.0 ± 1.0
Diboson	2.0 ± 2.0	-	-
total background	97 ± 12	24.4± 5.2	10.9 ± 3.4
$m(\tilde{\chi}_1^\pm/\tilde{\chi}_2^0, \tilde{\chi}_1^0) = (500, 310)$ GeV	20.7 ± 4.8	4.6 ± 2.3	1.0 ± 1.0
$m(\tilde{\chi}_1^\pm/\tilde{\chi}_2^0, \tilde{\chi}_1^0) = (800, 420)$ GeV	44.3 ± 2.3	33.6 ± 2.0	21.2 ± 1.6
$m(\tilde{\chi}_1^\pm/\tilde{\chi}_2^0, \tilde{\chi}_1^0) = (1000, 1)$ GeV	32.2 ± 1.8	31.9 ± 1.8	28.9 ± 1.7

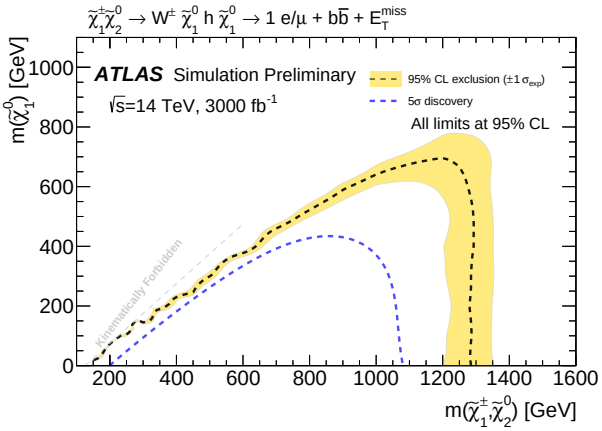

Figure 12: The 95% CL exclusion and discovery potential for $\tilde{\chi}_1^\pm\tilde{\chi}_2^0$ production at the HL-LHC (3000fb^{-1} at $\sqrt{s} = 14$ TeV), assuming $\tilde{\chi}_1^\pm \to W\tilde{\chi}_1^0$ and $\tilde{\chi}_2^0 \to h\tilde{\chi}_1^0$ with a branching ratio of 100%.

7 Conclusion

The large dataset of around 3000 fb^{-1} expected at the HL-LHC will significantly increase the ATLAS sensitivity to the productions of SUSY particles in the electroweak sector. This note summarises the expected sensitivities of direct productions of $\tilde{\tau}^+\tilde{\tau}^-$, $\tilde{\chi}_1^+\tilde{\chi}_1^-$, and $\tilde{\chi}_1^\pm\tilde{\chi}_2^0$ at the HL-LHC and the expected 95% exclusion regions and the 5σ discovery regions are summarised in Table 11. The discovery sensitivities of the HL-LHC are still rather limited in the challenging compressed region where mass differences between the NLSP and LSP are small. In particular, there is no discovery potential for the theoretically favoured stau co-annhilitation with small mass differences ($\Delta m(\tilde{\tau}, \tilde{\chi}_1^0) < 100$ GeV) or for the production of $\tilde{\tau}_R$ pairs. These challenging scenarios serve as ideal benchmarks for further improvements in the detector performance, reconstruction techniques and analysis methods at the HL-LHC.

SUSY particle	Final state	95% CL exclusion region for $m(\tilde{\chi}_1^0) = 0$ GeV	5σ discovery region for $m(\tilde{\chi}_1^0) = 0$ GeV
$\tilde{\tau}_L + \tilde{\tau}_R$	$\tau\tau$	< 730 GeV	[110, 530] GeV
$\tilde{\tau}_L$	$\tau\tau$	< 680 GeV	[110, 500] GeV
$\tilde{\tau}_R$	$\tau\tau$	< 420 GeV	
Wino $\tilde{\chi}_1^\pm$	WW-mediated 2ℓ	< 840 GeV	< 660 GeV
Wino $\tilde{\chi}_1^\pm, \tilde{\chi}_2^0$	WZ-mediated 3ℓ	< 1150 GeV	< 920 GeV
	Wh-mediated $1\ell bb$	< 1280 GeV	< 1080 GeV

Table 11: Summary of the 95% CL exclusion reach and the 5σ discovery reach at the end of HL-LHC for the direct productions of heavy SUSY partners in the electroweak sector, ssuming a massless $\tilde{\chi}_1^0$ LSP and baseline uncertainties. See text for the details of other assumptions of the signal models in each final state.

References

[1] Yu. A. Golfand and E. P. Likhtman,
Extension of the Algebra of Poincare Group Generators and Violation of p Invariance,
JETP Lett. **13** (1971) 323, [Pisma Zh. Eksp. Teor. Fiz. **13**, 452 (1971)].

[2] D. V. Volkov and V. P. Akulov, *Is the Neutrino a Goldstone Particle?*, Phys. Lett. B **46** (1973) 109.

[3] J. Wess and B. Zumino, *Supergauge Transformations in Four-Dimensions*,
Nucl. Phys. B **70** (1974) 39.

[4] J. Wess and B. Zumino, *Supergauge Invariant Extension of Quantum Electrodynamics*,
Nucl. Phys. B **78** (1974) 1.

[5] S. Ferrara and B. Zumino, *Supergauge Invariant Yang-Mills Theories*,
Nucl. Phys. B **79** (1974) 413.

[6] A. Salam and J. A. Strathdee, *Supersymmetry and Nonabelian Gauges*,
Phys. Lett. B **51** (1974) 353.

[7] G. R. Farrar and P. Fayet, *Phenomenology of the Production, Decay, and Detection of New Hadronic States Associated with Supersymmetry*, Phys. Lett. B **76** (1978) 575.

[8] ATLAS Collaboration, *The ATLAS Experiment at the CERN Large Hadron Collider*,
JINST **3** (2008) S08003.

[9] ATLAS Collaboration, *ATLAS Insertable B-Layer Technical Design Report*, ATLAS-TDR-019, 2010, URL: https://cds.cern.ch/record/1291633.

[10] ATLAS Collaboration, *Technical Design Report for the ATLAS Inner Tracker Pixel Detector*, ATLAS-TDR-030, 2017, URL: http://cdsweb.cern.ch/record/2285585.

[11] ATLAS Collaboration, *Technical Design Report for the ATLAS Inner Tracker Strip Detector*, ATLAS-TDR-025, 2017, URL: http://cdsweb.cern.ch/record/2257755.

[12] ATLAS Collaboration,
Technical Design Report for the Phase-II Upgrade of the ATLAS LAr Calorimeter,
ATLAS-TDR-027, 2017, URL: http://cdsweb.cern.ch/record/2285582.

[13] ATLAS Collaboration,
Technical Design Report for the Phase-II Upgrade of the ATLAS Tile Calorimeter,
ATLAS-TDR-028, 2017, URL: http://cdsweb.cern.ch/record/2285583.

[14] ATLAS Collaboration,
Technical Design Report for the Phase-II Upgrade of the ATLAS Muon Spectrometer,
ATLAS-TDR-026, 2017, URL: http://cdsweb.cern.ch/record/2285580.

[15] ATLAS Collaboration,
Technical Design Report for the Phase-II Upgrade of the ATLAS TDAQ System,
ATLAS-TDR-029, 2017, URL: http://cdsweb.cern.ch/record/2285584.

[16] ATLAS Collaboration, *ATLAS New Small Wheel Technical Design Report*, ATLAS-TDR-020,
2013, URL: https://cds.cern.ch/record/1552862.

[17] J. Linnemann, *Measures of Significance in HEP and Astrophysics*, 2003,
arXiv: 0312059 [physics].

[18] M. Baak et al., *HistFitter software framework for statistical data analysis*,
Eur. Phys. J. C **75** (2015) 153, arXiv: 1410.1280 [hep-ex].

[19] G. Cowan, K. Cranmer, E. Gross and O. Vitells,
Asymptotic formulae for likelihood-based tests of new physics, Eur. Phys. J. C **71** (2011) 1554,
arXiv: 1007.1727 [physics.data-an].

[20] A. L. Read, *Presentation of search results: The CL(s) technique*, J. Phys. G **28** (2002) 2693.

[21] ATLAS Collaboration,
Expected performance for an upgraded ATLAS detector at High-Luminosity LHC,
ATL-PHYS-PUB-2016-026, 2016, URL: https://cds.cern.ch/record/2223839.

[22] J. Alwall et al., *The automated computation of tree-level and next-to-leading order differential cross sections, and their matching to parton shower simulations*, JHEP **07** (2014) 079,
arXiv: 1405.0301 [hep-ph].

[23] T. Sjöstrand et al., *An Introduction to PYTHIA 8.2*, Comput. Phys. Commun. **191** (2015) 159,
arXiv: 1410.3012 [hep-ph].

[24] ATLAS Collaboration, *ATLAS Pythia 8 tunes to 7 TeV data*, ATL-PHYS-PUB-2014-021, 2014,
URL: https://cds.cern.ch/record/1966419.

[25] S. Carrazza, S. Forte and J. Rojo, 'Parton Distributions and Event Generators',
Proceedings, 43rd International Symposium on Multiparticle Dynamics (ISMD 13), 2013 89,
arXiv: 1311.5887 [hep-ph],
URL: https://inspirehep.net/record/1266070/files/arXiv:1311.5887.pdf.

[26] L. Lönnblad and S. Prestel, *Merging Multi-leg NLO Matrix Elements with Parton Showers*,
JHEP **03** (2013) 166, arXiv: 1211.7278 [hep-ph].

[27] B. Fuks, M. Klasen, D. R. Lamprea and M. Rothering,
Gaugino production in proton-proton collisions at a center-of-mass energy of 8 TeV,
JHEP **10** (2012) 081, arXiv: 1207.2159 [hep-ph].

[28] B. Fuks, M. Klasen, D. R. Lamprea and M. Rothering, *Precision predictions for electroweak superpartner production at hadron colliders with Resummino*, Eur. Phys. J. C **73** (2013) 2480,
arXiv: 1304.0790 [hep-ph].

[29] C. Borschensky et al.,
Squark and gluino production cross sections in pp collisions at $\sqrt{s}$ = 13, 14, 33 and 100 TeV,
Eur. Phys. J. C **74** (2014) 3174, arXiv: 1407.5066 [hep-ph].

[30] T. Gleisberg et al., *Event generation with SHERPA 1.1*, JHEP **02** (2009) 007, arXiv: 0811.4622 [hep-ph].

[31] D. J. Lange, *The EvtGen particle decay simulation package*, Nucl. Instrum. Meth. A **462** (2001) 152.

[32] S. Alioli, P. Nason, C. Oleari and E. Re, *A general framework for implementing NLO calculations in shower Monte Carlo programs: the POWHEG BOX*, JHEP **06** (2010) 043, arXiv: 1002.2581 [hep-ph].

[33] T. Sjostrand, S. Mrenna and P. Z. Skands, *A Brief Introduction to PYTHIA 8.1*, Comput. Phys. Commun. **178** (2008) 852, arXiv: 0710.3820 [hep-ph].

[34] R. D. Ball et al., *Parton distributions for the LHC Run II*, JHEP **04** (2015) 040, arXiv: 1410.8849 [hep-ph].

[35] T. Sjostrand, S. Mrenna and P. Z. Skands, *PYTHIA 6.4 Physics and Manual*, JHEP **05** (2006) 026, arXiv: hep-ph/0603175.

[36] P. Z. Skands, *Tuning Monte Carlo Generators: The Perugia Tunes*, Phys. Rev. D **82** (2010) 074018, arXiv: 1005.3457 [hep-ph].

[37] H.-L. Lai et al., *New parton distributions for collider physics*, Phys. Rev. D **82** (2010) 074024.

[38] ATLAS Collaboration, *Measurement of the Z/γ^* boson transverse momentum distribution in pp collisions at $\sqrt{s} = 7$ TeV with the ATLAS detector*, JHEP **09** (2014) 145, arXiv: 1406.3660 [hep-ex].

[39] ATLAS Collaboration, *Summary of ATLAS Pythia 8 tunes*, ATL-PHYS-PUB-2012-003, 2012, URL: https://cds.cern.ch/record/1474107.

[40] K. Griest and D. Seckel, *Three exceptions in the calculation of relic abundances*, Phys. Rev. D **43** (10 1991) 3191.

[41] G. Hinshaw et al., *Nine-Year Wilkinson Microwave Anisotropy Probe (WMAP) Observations: Cosmological Parameter Results*, Astrophys. J. Suppl. **208** (2013) 19.

[42] A. Djouadi et al., 'The Minimal supersymmetric standard model: Group summary report', *GDR (Groupement De Recherche) - Supersymetrie Montpellier, France, April 15-17, 1998*, 1998, arXiv: hep-ph/9901246 [hep-ph], URL: https://inspirehep.net/record/481987/files/arXiv:hep-ph_9901246.pdf.

[43] ATLAS Collaboration, *Search for the electroweak production of supersymmetric particles in $\sqrt{s} = 8$ TeV pp collisions with the ATLAS detector*, Phys. Rev. D **93** (2016) 052002, arXiv: 1509.07152 [hep-ex].

[44] CMS Collaboration, *Search for supersymmetry in events with a τ lepton pair and missing transverse momentum in proton-proton collisions at $\sqrt{s} = 13$ TeV*, (2018), arXiv: 1807.02048 [hep-ex].

[45] ATLAS Collaboration, *Search for the direct production of charginos and neutralinos in final states with tau leptons in $\sqrt{s} = 13$ TeV pp collisions with the ATLAS detector*, Eur. Phys. J. C **78** (2018) 154, arXiv: 1708.07875 [hep-ex].

[46] M. Cacciari, G. P. Salam and G. Soyez, *The anti-k_t jet clustering algorithm*, JHEP **04** (2008) 063, arXiv: 0802.1189 [hep-ph].

[47] M. Cacciari and G. P. Salam, *Dispelling the N^3 myth for the k_t jet-finder*, Phys. Lett. B **641** (2006) 57, arXiv: hep-ph/0512210 [hep-ph].

[48] C. G. Lester and D. J. Summers,
Measuring masses of semiinvisibly decaying particles pair produced at hadron colliders,
Phys. Lett. B **463** (1999) 99, arXiv: hep-ph/9906349 [hep-ph].

[49] A. Barr, C. Lester and P. Stephens, *m(T2): The Truth behind the glamour*,
J. Phys. G **29** (2003) 2343, arXiv: hep-ph/0304226 [hep-ph].

[50] R. Barbieri and G. F. Giudice, *Upper Bounds on Supersymmetric Particle Masses*,
Nucl. Phys. B **306** (1988) 63.

[51] B. de Carlos and J. A. Casas, *One loop analysis of the electroweak breaking in supersymmetric models and the fine tuning problem*, Phys. Lett. B **309** (1993) 320,
arXiv: hep-ph/9303291 [hep-ph].

[52] ATLAS Collaboration,
Search for direct production of charginos, neutralinos and sleptons in final states with two leptons and missing transverse momentum in pp collisions at $\sqrt{s} = 8$ *TeV with the ATLAS detector*,
JHEP **05** (2014) 071, arXiv: 1403.5294 [hep-ex].

[53] ATLAS Collaboration, *Search for direct chargino pair production with W-boson mediated decays in events with two leptons and missing transverse momentum in the final state at* $\sqrt{s} = 13$ *TeV with the ATLAS detector.*, ATLAS-CONF-2018-042, 2018,
URL: http://cdsweb.cern.ch/record/2632578.

[54] M. Carena, S. Heinemeyer, O. Stål, C. E. M. Wagner and G. Weiglein, *MSSM Higgs Boson Searches at the LHC: Benchmark Scenarios after the Discovery of a Higgs-like Particle*,
Eur. Phys. J. C **73** (2013) 2552, arXiv: 1302.7033 [hep-ph].

[55] ATLAS Collaboration, *Observation of a new particle in the search for the Standard Model Higgs boson with the ATLAS detector at the LHC*, Phys. Lett. B **716** (2012) 1,
arXiv: 1207.7214 [hep-ex].

[56] CMS Collaboration,
Observation of a new boson at a mass of 125 GeV with the CMS experiment at the LHC,
Phys. Lett. B **716** (2012) 30, arXiv: 1207.7235 [hep-ex].

[57] ATLAS and CMS Collaborations,
Measurements of the Higgs boson production and decay rates and constraints on its couplings from a combined ATLAS and CMS analysis of the LHC pp collision data at $\sqrt{s} = 7$ *and* 8 *TeV*,
ATLAS-CONF-2015-044, 2015, URL: https://cds.cern.ch/record/2052552.

[58] ATLAS Collaboration, *Search for electroweak production of supersymmetric particles in final states with two or three leptons at* $\sqrt{s} = 13$ *TeV with the ATLAS detector*, (2018),
arXiv: 1803.02762 [hep-ex].

[59] ATLAS Collaboration, *Search for electroweak production of supersymmetric states in scenarios with compressed mass spectra at* $\sqrt{s} = 13$ *TeV with the ATLAS detector*,
Phys. Rev. D **97** (2018) 052010, arXiv: 1712.08119 [hep-ex].

[60] ATLAS Collaboration, *Search for chargino-neutralino production using recursive jigsaw reconstruction in final states with two or three charged leptons in proton-proton collisions at* $\sqrt{s} = 13$ *TeV with the ATLAS detector*, Phys. Rev. D **98** (2018) 092012,
arXiv: 1806.02293 [hep-ex].

[61] ATLAS Collaboration, *Prospect for a search for direct pair production of a chargino and a neutralino decaying via aW boson and the lightest Higgs boson in final states with one lepton, two b-jets and missing transverse momentum at the high luminosity LHC with the ATLAS Detector*, ATL-PHYS-PUB-2015-032, 2015, URL: https://cds.cern.ch/record/2038565.

[62] D. R. Tovey,
On measuring the masses of pair-produced semi-invisibly decaying particles at hadron colliders, JHEP **04** (2008) 034, arXiv: 0802.2879 [hep-ph].

[63] G. Polesello and D. R. Tovey,
Supersymmetric particle mass measurement with the boost-corrected contransverse mass, JHEP **03** (2010) 030, arXiv: 0910.0174 [hep-ph].